AN ABSTRACT OF THE THESIS OF

Peter M. Anthoni for the degree of Master of Science in Physics presented on May 2, 1996. Title: Carbon Dioxide Eddy Flux Measurements in Complex Terrain from a Coniferous Forest under the Influence of Marine Air.

Abstract approv[redacted] Redacted for Privacy

Richard J. Vong

Measurements of the carbon dioxide net exchange were made during Summer 1994 for a coniferous forest consisting primarily of Pacific silver fir (*Abies amabilis*) and Western hemlock (*Tsuga heterophylla*). The research site was located on the Olympic Peninsula in Washington in complex terrain at the top of Cheeka Peak (elevation 463 m), where prevailing Southwest winds bring marine air 4 km inland from the Pacific Ocean.

The net CO_2 exchange of a terrestrial ecosystem is determined by two processes: photosynthetic uptake of CO_2 and respiratory release of CO_2. For homogenous and steady-state conditions, the net CO_2 exchange can be derived from the eddy correlation technique, where three dimensional wind speed and carbon dioxide gas concentration are measured simultaneously. The net flux towards or from the canopy is the time-averaged covariance of the wind speed component normal to the streamlines and the measured CO_2 concentration.

The responses of the photosynthesis dominated daytime downward CO_2 flux to incoming "photosynthetically active radiation" (PAR) and water vapor pressure deficit (VPD) were determined. The dependence of nighttime respiration (upward carbon dioxide flux) on soil temperature was investigated.

A clear relation between incident PAR and daytime net CO_2 uptake was found. During 24-hour periods with high midday photosynthetically active

radiation (PAR > 1200 μmol m^{-2} s^{-1}) the net carbon fixation by the forest was about 23.3 kg-carbon ha^{-1} day^{-1}. Days with reduced incoming radiation (600 μmol m^{-2} s^{-1}< PAR < 1200 μmol m^{-2} s^{-1}) due to cloud cover resulted in a lower net fixation of 10.5 kg-carbon ha^{-1} day^{-1}. For days with a substantial decrease of incident PAR (PAR < 600 μmol m^{-2} s^{-1}) throughout the day due to persistent surface or low level cloud at the site, a net release of carbon of 6.5 kg-carbon ha^{-1} day^{-1} was found.

A reduction in the photosynthetic rate due to water vapor pressure deficit was not observed, probably because the moist marine air from the Pacific Ocean leads to saturation deficit generally below 6.5 hPa, too small to cause a significant leaf stomata closure. The narrow soil temperature range of 10 °C to 14.5 °C throughout the experiment made any dependence of nighttime respiration on temperature undetectable.

Overall, it was shown that the eddy correlation technique is suitable to evaluate the carbon dioxide exchange of a forest located in complex terrain. As expected, the derived eddy CO_2 flux was clearly correlated with the amount of incident photosynthetically active radiation. The forest at Cheeka Peak accumulated carbon from the atmosphere for days with conditions of high or mid-range incoming PAR, and only for days with persistent surface or low level cloud throughout the day was a net release of carbon detected.

Carbon Dioxide Eddy Flux Measurements in Complex Terrain from a Coniferous Forest under the Influence of Marine Air

by

Peter M. Anthoni

A THESIS

submitted to

Oregon State University

in partial fulfillment of

the requirements for the

degree of

Master of Science

Presented May 2, 1996

Commencement June 1997

Master of Science thesis of Peter M. Anthoni presented on May 2, 1996

APPROVED:

Redacted for Privacy

Major Professor, representing Physics

Redacted for Privacy

Head of Department of Physics

Redacted for Privacy

Dean of Graduate School

I understand that my thesis will become part of the permanent collection of Oregon State University libraries. My signature below authorizes release of my thesis to any reader upon request.

Redacted for Privacy

Peter M. Anthoni, Author

ACKNOWLEDGEMENT

I want to thank my parents, Fritz and Hildegard Anthoni, who encouraged me to go on with my studies. Special thanks to my brother Klaus and my sisters Gaby and Anette who I love very much.

Special thanks go to Dave Covert for the use of his site, tower, and facilities and for all of his help with setting up the CACHE project. I thank the entire ASTER facility group for making CACHE-3 work: Tom Horst, Kurt Knudson, Charlie Martin, John Militzer, Santiago Newbery, Steve Oncley, Steve Semmer, and Lou Verstraete. Special thanks to Tony Delany for setting up the gas analyzer system. Thanks also are due to Gordon MacLean for his support and for being readily available for troubleshooting problems with the ASTER computer system. I thank Lee Klinger for classifying the forest at Cheeka peak.

I would like to thank my advisor, Richard Vong, for his guidance and long lasting support throughout my studies, for bearing with my *German-English* and handing me various ideas to improve it. Thanks are due to Mike Unsworth and Beverly Law for useful discussions and suggestions to improve my work.

I want to thank Andy Kowalski, a good friend and colleague graduate student, for his help in the project and in my life. I would like to thank my housemates, Stephanie, Kim, Will, Katie and Vaneska, for being friends and keeping up with my unusual work hours.

This work was supported by the National Science Foundation grant #ATM9118316 (Atmospheric Chemistry desk) and funding from the Center for Analysis of Environmental Change.

TABLE OF CONTENTS

TABLE OF CONTENTS (Continued)

TABLE OF CONTENTS (Continued)

LIST OF FIGURES

LIST OF FIGURES (Continued)

LIST OF TABLES

LIST OF APPENDIX FIGURES

LIST OF APPENDIX TABLES

LIST OF ABBREVIATIONS

Name	Description
$\overline{u'_i C'}$	turbulent eddy flux of C in i^{th} direction (mol m^{-2} s^{-1} or kg-C m^{-2} s^{-1})
$\overline{u'_i u'_j}$	turbulent eddy flux of u_j momentum in the i^{th} direction
$(CH_2O)_6$	Glucose
Abam	*Abies amabilis* (Pacific Silver Fir)
BA	basal area (kg m^{-2}) subscripts: Ba_t total; Ba_{as} species specific
C	specific heat capacity (J kg^{-1} K^{-1}) subscripts: C_p at constant pressure, C_v at constant volume
C	speed of sound in air (m s^{-1})
C	tracer concentration (kg m^{-3} or mol m^{-3})
c	tracer mixing ratio (mass of C per unit mass of air)
CH_2O	carbohydrate
CO_2	carbon dioxide
dbh	tree diameter measured at breast height (~1.5 m)
e	base for natural logarithm (2.71828)
e	water vapor pressure (Pa) subscripts: e_a in the bulk air; e_s saturation
F	turbulent eddy flux subscripts: F_{CO2} carbon dioxide flux (μmol m^{-2} s^{-1} or mg-C m^{-2} s^{-1}); F_{max} maximum attainable carbon dioxide flux
G	soil heat storage or heat loss by conduction (W m^{-2})
GMT	Greenwich mean time
H	sensible heat flux (W m^{-2})
H_2O	water molecule
IPAR	incoming PAR (μmol m^{-2} s^{-1})
k	extinction coefficient subscripts: k_w for water vapor, k_o for oxygen
LAI	leaf area index (dimensionless) subscripts: LAI_s species specific, LAI_{as} above shrub layer
LBM	green leaf dry biomass (kg m^{-2}) subscript: LBM_s species specific
LE	latent heat flux (W m^{-2})
LWC	cloud liquid water content (g m^{-3})
M	molecular weight (g mol^{-1})
mol	mole (amount of substance containing Avogadro's number of particles)
MSL	mean sea level

LIST OF ABBREVIATIONS (Continued)

Name	Description
O_2	oxygen
P	photosynthesis
P	pressure (Pa)
PAR	photosynthetically active radiation (μmol m^{-2} s^{-1}) ;400 to 700 nm
PDT	Pacific daylight savings time (GMT -07:00)
R	electrical resistance (Ω) subscripts: R_T at temperature T, R_o at temperature T_o
R	respiration subscripts: R_d dark; R_g growth; R_m maintenance; R_o rate at T = 0 °C
R	universal gas constant (J mol^{-1} K^{-1})
T	temperature (K or °C) subscripts: T_l leaf; T_s soil
t	time (s)
Thpl	*Thuja plicata* (Red Cedar)
Tshe	*Tsuga heterophylla* (Western hemlock)
T_v	virtual temperature (K or °C)
u	windspeed in x-direction (m s^{-1}) superscript: u* friction velocity, u_i i^{th} component; u_1 x-component; u_2 y-component; u_3 z-component
V	volume (m^3)
V	electric voltage (V)
v	windspeed in y-direction (m s^{-1})
VPD	water vapor pressure deficit (Pa)
w	windspeed in z-direction (m s^{-1})
x	distance (m)
y	distance (m)
z	distance, height, elevation (m)
α	contact angle (degree or radian)
α_p	quantum use efficiency in mol mol^{-1}
β	exponential curve shape factor
λ	latent heat of evaporation (J kg^{-1})
η	azimuthal rotation angle (degree or radian)
θ	vertical rotation angle (degree or radian)
ρ	density (kg m^{-3}) subscripts: ρ_a air; ρ_{CO2} carbon dioxide

LIST OF ABBREVIATIONS (Continued)

Name	Description
$( )'$	deviation from the mean value
$\overline{( )}$	average operator
∂	partial derivative
$\overline{a'b'}$	covariance of a and b
Σ	summation

Carbon Dioxide Eddy Flux Measurements in Complex Terrain from a Coniferous Forest under the Influence of Marine Air

1. Introduction

1.1 Background

The carbon dioxide net exchange of a plant-soil ecosystem is determined by two processes:

1) Photosynthesis (P): uptake of CO_2

2) Respiration (R): release of CO_2

Photosynthesis is the transformation of CO_2 into complex organic molecules with the aid of energy from sun light. The overall chemical reaction of photosynthesis is given by

$$CO_2 + H_2O + h\nu \rightarrow (CH_2O) + O_2 \qquad (1)$$

For every molecule of carbohydrate (CH_2O) produced, one molecule of oxygen (O_2) is released and one molecule of carbon dioxide (CO_2) and water (H_2O) is removed, where the process energy is supplied by the absorbed radiation ($h\nu$). The wavelengths at which photosynthesis is most efficient are from 400 to 700 nm (from blue through green to red), the visible part of the radiation spectrum (Jones, 1992). Due to plant photosynthetic activity in this wavelength regime it is also termed "photosynthetically active radiation (PAR)".

Respiration releases the energy stored in carbohydrates by the oxidation of the carbohydrates to carbon dioxide and water. The CO_2 released during this process can be attributed to the decomposition of dead organic matter by microorganisms, and the growth and maintenance respiration from the plant tops and roots. The growth component (R_g) of plant respiration is used for growing and synthesizing new tissue, where as the maintenance part (R_m) provides the

energy to support the existing cells of the plant. The overall chemical reaction for respiration is given by

$$\text{Glucose } (CH_2O)_6 + 6\,O_2 \rightarrow 6\,CO_2 + 6\,H_2O + \text{energy} \qquad (2)$$

The plant's metabolism is strongly coupled to meteorological and physiological controlling factors. The major factor controlling photosynthesis is the input of usable photosynthetically active radiation. The amount of intercepted and absorbed radiation is dependent on the leaf area and leaf distribution in the forest canopy. Landsberg (1986) presents a widely used empirical relationship for CO_2 uptake of plants as a function of incident PAR,

$$F = \frac{\alpha_p F_{max} PAR}{\alpha_p PAR + F_{max}} + R_d \qquad (3)$$

where F is the net CO_2 uptake, F_{max} is the maximum attainable uptake, α_p is the quantum use efficiency (mole of CO_2 per mole of photons), PAR is the incident photosynthetically active radiation, and R_d is a respiration term.

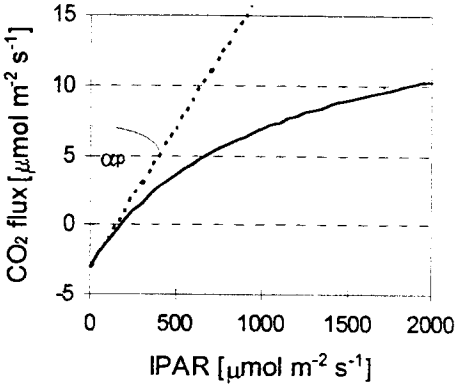

Figure 1.1 Example Landsberg model light response curve

For low incident PAR values a rapid increase in CO_2 uptake is expected, where the initial slope of the response curve is the quantum use efficiency α_p. In the high PAR region the photosynthetic process becomes saturated due to limits on the regeneration rate of a catalytic enzyme (ribulose-biphosphate RuBP), and the response curve levels out at the maximum attainable carbon uptake rate F_{max}. In the limit of zero photosynthetically active radiation the light response curve crosses the CO_2 flux axis at the dark respiration value R_d. Figure 1.1 shows a Landsberg model curve with the parameters α_p = 0.02 mol mol^{-1}, F_{max} = 20 μmol m^{-2} s^{-1}, R_d = -3.0 μmol m^{-2} s^{-1} (curve is shown with plant physiological sign convention; upward respiratory flux negative and photosynthetically-driven downward flux positive).

Furthermore, photosynthetic carbon uptake is constrained by the leaf-to-air water vapor pressure deficit and plant water stress. The water vapor pressure deficit (VPD) is defined by the difference in the actual water vapor pressure (e_a) of the air and saturation water vapor pressure ($e_s(T_l)$) at leaf temperature,

$$VPD = e_s(T_l) - e_a \tag{4}$$

At large leaf-to-air vapor pressure deficits the stomatal pores of leaves close to prevent the plant from losing excess water due to the increased evaporative demand (Monteith and Unsworth, 1990; Jones, 1992), and this closure decreases the stomatal conductance. Because carbon assimilation is positively coupled with stomatal conductance (Landsberg, 1986), this decrease leads to a reduction in CO_2 uptake. Plant water stress has less effect on the carbon uptake reduction as long as the water status does not fall below a certain threshold (Landsberg, 1986). The threshold value strongly depends on leaf-age and adaptation of the plants to drought occurrences.

The respiration rate is strongly dependent on temperature. Respiration increases exponentially with temperature (Jarvis and Leverenz, 1983; Ryan, 1991):

$$R = R_o e^{\beta T} \tag{5}$$

where R_o is the respiration rate at T = 0 °C, β is an exponential curve shape parameter, and T is the temperature in °C.

The CO_2 net exchange of a plant community is determined by the net of photosynthesis and respiration processes. During daytime, photosynthesis usually exceeds respiration and the canopy is a sink for carbon dioxide. Turbulent mixing in the atmosphere brings CO_2-rich air from above the canopy downward into the forest and CO_2 depleted air from the canopy region is mixed upward. A net downward carbon dioxide flux into the forest layer can be observed, due to the dominance of photosynthesis over respiration. During nighttime no photosynthesis occurs and the forest and soils release CO_2 from respiration. At night the forest is a source for atmospheric carbon dioxide. Under turbulent conditions the respired CO_2 is transported upward and air with lower carbon dioxide concentration is mixed downward, which manifests as a net CO_2 flux out of the forest. For stable conditions during the night the upward transport can be suppressed and an accumulation of carbon dioxide in the forest layer can occur.

Net fluxes in the surface layer are measured with the eddy correlation technique. The technique is a commonly used micrometeorological method that provides a direct measurement of the net flux in the surface layer, for example sensible and latent heat fluxes, momentum flux, or carbon dioxide flux. The method calculates the flux from fast response sample data as the time-averaged covariance between the wind component normal to the wind streamlines and a scalar quantity, such as temperature, water vapor, momentum, or carbon dioxide.

The eddy correlation technique used to measure the net CO_2 exchange of a forest ecosystem has the advantages of being "in situ", i.e. it does not disturb the environment of the plant canopy, and the time-averaged measurement at a point provides an area-integrated measurement of exchange rates between the surface and the atmosphere (Baldocchi et al., 1988). Under ideal conditions (horizontally uniform and level surface, no sources or sinks in the atmosphere

above the surface, steady-state of the constituent concentration) the vertical turbulent flux (F) of a constituent is given by

$$F = \overline{\rho_a}\,\overline{w'c'} \qquad (6)$$

where $\overline{\rho_a}$ is the mean density of dry air, $\overline{w'c'}$ is the covariance of the vertical wind speed (w) and the mixing ratio (c) of the constituent (mass of C per unit mass of dry air); for $F < 0$ the flux is directed downward while for $F > 0$ the flux is directed upward (Baldocchi et al., 1988).

To use the eddy correlation technique in complex terrain, coordinate rotations of the three wind speed components are necessary to remove mean vertical velocities introduced by terrain inhomogeneity and imperfect alignment of the sensor with the slope (McMillen, 1988; Baldocchi et al., 1988). For sloping terrain < 8-15%, reliable turbulent fluxes perpendicular to the streamline can be obtained due to coordinate rotations (Baldocchi et al., 1988).

The turbulent fluctuations superimposed on the mean wind, eddies, act as the carriers for the transfer of the constituent. The time response of the measurement system has to be sufficiently fast to resolve the entire scale range of the transporting eddies. The necessary instrument response time primarily depends on the height above the surface and the wind speed. The sensor frequency response for neutral conditions should be at least in the order of $2\,u\,z^{-1}$, where u is the wind speed, and z is height above the local displacement level (McMillen, 1988). For the conditions at Cheeka Peak with $z \approx 5$ m (measurement level at 10 m with an average tree height of 6 m) and a typical wind speed of $u = 5$ m s^{-1} a sampling frequency of about 2 Hz or higher would be adequate.

The eddy correlation technique is increasingly used to evaluate CO_2 exchange of forest ecosystems. Various short term and long term studies were performed throughout the past years including: Verma et al. (1986) over a fully-leafed deciduous forest in Eastern Tennessee, Wofsy et al. (1993) and Goulden

et al. (1995; 1996b) at Harvard Forest in Massachusetts, Hollinger et al. (1994) at an undisturbed old-growth temperate forest, Fan et al. (1995) and Goulden et al. (1996a) at a boreal lichen woodland in Canada, and Grace et al. (1995a, 1995b) at a tropical rain forest in the Amazon.

During Summer 1994, the third field intensive campaign of the NSF-funded Cloud and Aerosol CHemistry Experiment (CACHE) took place on the Olympic Peninsula, Washington. From August 8 to September 23, 1994 (Julian days 220 to 266) the Atmosphere-Surface Turbulent Exchange Research Facility (ASTER) from the National Center of Atmospheric Research (NCAR) was operational at the University of Washington research station on top of Cheeka Peak, a ridge near the coast of the Pacific Ocean. As a part of the system, a closed-path infrared gas analyzer (IRGA) was operated next to a sonic anemometer to evaluate the carbon dioxide exchange from the mid-latitude forest at Cheeka Peak with the eddy correlation technique.

The location close to the Pacific Ocean and the prevailing South-West winds result in a frequent input of marine air at the research site. Under those conditions a constraint on the carbon uptake due to water stress or leaf-to-air water vapor pressure deficit is not expected. Orographically driven lifting of the moist marine air results in frequent low level cloud occurrence at the site. The low level clouds, obscuring the sun, should lead to a reduction in incident photosynthetically active radiation and, consequently, be reflected in a lower photosynthetic rate of the forest.

The goals of this study are

1) to demonstrate the applicability of the eddy correlation technique for measuring the CO_2 net exchange of a forest ecosystem located in complex terrain.
2) to investigate the response of the Pacific silver fir forest to environmental factors (PAR, δe, T) that are themselves controlled by the marine influence and complex topography.

1.2 Site Description

The field experiment was performed at the aerosol research site of the University of Washington in the North-West extremity of the Olympic Peninsula, Washington at latitude 124° 37' 30" W, and longitude 48° 17' 56" N (see Figure 1.2 and Figure 1.3). The research site is located in complex terrain on top of Cheeka Peak (elevation 463 m) in the coast range about 11 km from the closest town, Neah Bay. The hill top lies about 4 km inland from Anderson Point at the coast of the Pacific Ocean. The experimental site occupies the flat top at the South end of a North-South extending ridge. The terrain falls off steeply to the East, South and West with an average slope of about 17°. The terrain on the West-Southwest sector of the mountain is fairly homogeneous, descending with some smaller rolling hill sections. To the South and Northwest are some lower elevation hills. The area from the ocean to the ridge base is generally flat with some smaller ridges (less than 150 m).

The forested slopes around Cheeka Peak were logged in 1964-65 and replanted with a mixture of coniferous trees. Tree species found are Pacific Silver Fir (*Abies amabilis*), Western Hemlock (*Tsuga heterophylla*), and minor occurrence of Red Cedar (*Thuja plicata*) and Sitka Spruce (*Picea sitchensis*). The average age of the Fir and Hemlock trees close to the hill top was 25 years in 1994. The understory consists mostly of Salal (*Gaulteria shallon)*, an ericaceous shrub.

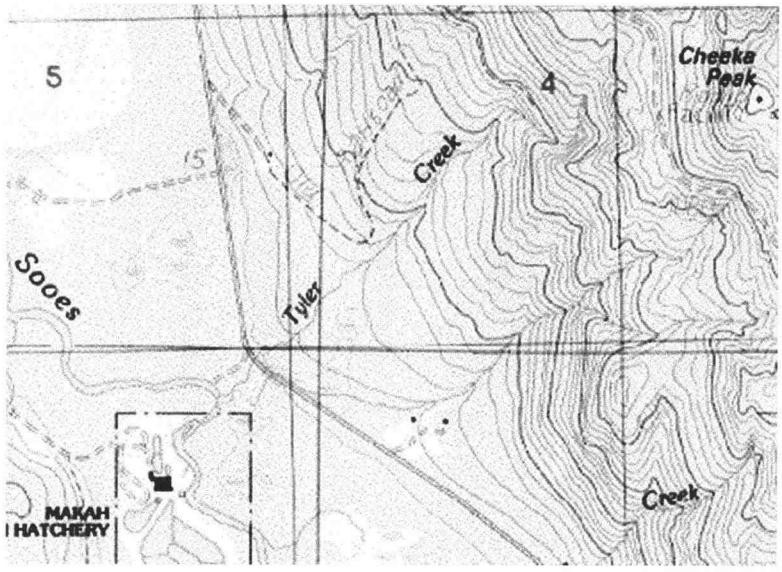

Figure 1.2 Topographic map with the CACHE research site on top of Cheeka Peak showing the South-West sector of the hill (Cheeka Peak is located in the top right corner of the map)

Figure 1.3 Picture of the South-West slope at Cheeka Peak (picture was taken facing in the South-East direction)

2. Methods

2.1 Forest Specification

A 10 m wide and 100 m long belt transect was setup down into the canopy starting from the flux measurement tower in the direction of the prevailing South-West winds (240 °). The transect was divided into 10 plots (10 by 10 m in size), where the distances were determined using tape measures. On August 1-3, 1994 each plot in the transect was sampled for slope, elevation, species identification, tree diameter at breast height (dbh @~1.5 m), tree height, sapling count, leaf area index, and percent cover of the dominant growth forms (deciduous shrubs, ericaceous shrubs, forbs, graminoids, and mosses). Trees with a smaller than 4 cm dbh and height taller than 1.5 m were counted as saplings. Trees with dbh greater than 4 cm counted as trees. The slope of the plot and the tree height were measured with a clinometer, and the elevation was determined with an altimeter. Leaf area index (LAI) measurements (total projected leaf area per unit area of ground) were performed with a Licor LAI-2000 meter, which measures the gap fraction of the canopy (Chason et al., 1991; Jones, 1992). For each plot four LAI readings were obtained, two above the existing shrub layer and two below. The percentage cover of dominant growth forms was estimated visually.

Two branches of each of the major forest species in the transect Pacific silver fir, Western hemlock, Red cedar, and Salal were collected and packaged for laboratory analysis of leaf area and leaf dry mass. In the lab, the leaves were removed from the branches and leaf area was determined with a leaf area meter, by measuring the projected area of the removed leaves. The leaves were dried for 24 hours at 50 °C and weighed to obtain the leaf dry mass.

The basal area of an individual tree (BA_i) was computed according to

$$BA_i = \pi\left(\frac{dbh}{2}\right)^2 \quad (7)$$

where dbh is the measured diameter at breast height. The basal area of a species (BA_s) in a plot is the sum of all individual BA_i expressed on a per area basis.

The leaf area index of a species (LAI_s) was determined as the fraction of above-shrub layer leaf area index (LAI_{as}), weighted by the species fraction of total plot basal area (BA_t)

$$LAI_s = LAI_{as}\left(\frac{BA_s}{BA_t}\right) \quad (8)$$

The green leaf dry biomass for a given species (LBM_s) was computed according to

$$LBM_s = LAI_s\ SLM \quad (9)$$

where SLM is specific leaf mass.

The total leaf surface area is twice the LAI_s of a species, due to the essentially flat structure of the leaves of all the dominant species.

2.2 Experimental Setup

Instruments were mounted on 4 towers located at the West facing edge of the flat crest: one walk-up tower (Walk) on top of a UW instrument container (total height ~10 m), the other three towers were of the low-profile type (Psyc, Prop and Flux) with heights 10 m, 15 m and 15 m. The Walk tower was separated from the other towers by 6 m (Psyc), 9 m (Prop), and 26 m (Flux). A radiation stand (Darkhorse) was setup within the canopy on the southern slope of the ridge. Access to Darkhorse was obtained by cutting a 15 m long trail down the south slope. The cross beam of the stand was oriented in the East-West

direction, level within a few degrees, and approximately 1 m above the 3 m deep vegetation, mainly consisting of Salal shrubs and Pacific silver fir.

At 10 m on the Walk tower a cloud water sampler was operated to collect cloud samples, and a 3 m long boom (rotatable into the mean wind) was instrumented with fast response sensors. An Applied Technology Instrumentation (ATI) sonic anemometer model SWS-211/3K and a Solent Research Grade sonic measured the three dimensional wind speed, the sampling tube of a closed-path non-dispersive infrared gas analyzer and a platinum resistance temperature probe were co-located with the ATI sonic. An aspirated forward scattering spectrometer (PMS model FSSP-100) measured cloud droplet size spectra and droplet concentration. The Psyc tower supported NCAR psychrometer probes to measure temperature and humidity profiles at heights 2.5, 5, 7.5, and 10 m above ground level (agl). A NCAR barometric pressure sensor was operated next to the 2.5 m psychrometer. On the Prop tower 6 NCAR prop-vanes were installed at levels from 2.5 m to 15 m to measure the horizontal wind speed and wind direction. The 12.5 m and 15 m levels were supplemented with NCAR psychrometer probes. The Flux tower was instrumented at 10 m and 15 m, with an ATI sonic anemometer, and fast response sensors for cloud liquid water content (Gerber Particle Volume Monitor PVM-100), temperature (Atmospheric Instrumentation Research Inc. platinum resistance temperature probe), and water vapor concentration (Campbell Scientific Kr Hygrometer).

Radiation measurements included net radiation with a Micromet Systems Net Radiometer Q5, upward and downward short wave radiation with two Eppley Precision Spectral Pyranometers, upward and downward long wave radiation with two Eppley Precision Spectral Pyrgeometers, and photosynthetically active radiation (PAR; 400-700 nm) with three Licor Quantum 190AS sensors. The PAR sensors were originally placed in the canopy at the Southern edge of the hilltop one facing upward in the open for measurement of incident PAR, the other two below the branches of a Silver fir tree. On Julian-day 236 (August, 24th) the

sensors were moved in a more representative location on and below the Darkhorse, one facing upward in the open, and one facing downward, and located 1 m from the radiation stand crossbeam. The third sensor was placed on the ground below the canopy around the radiation stand.

Soil measurements were performed in the vicinity of the canopy around the radiation stand with multiplexed NCAR thermocouple temperature probes and Micromet Systems soil heat flux plates. The thermocouple temperature probes were placed at soil depth 1, 3, 5, and 7 cm. The soil heat flux plates were near the temperature sensors at a depth of 8 cm.

2.3 Instruments

2.3.1 CO_2 Gas Analyzer

The carbon dioxide instrument is a differential, non-dispersive, closed-path infrared gas analyzer (IRGA; Licor model LI-6251) with an instrument response time of 0.1 seconds. The measurement principle is based on the absorption of IR radiation by carbon dioxide. The gas concentration is determined by the difference in absorption in two sampling cells. The reference cell contains a gas with known CO_2 concentration and the sample cell contains a gas with unknown concentration. Infrared radiation is passed through both cells and the analyzer output is proportional to the absorption difference between the cells. The cross sensitivity to other gases (e.g. H_2O) is minimized by the use of a bandpass optical filter tuned to the 4.26 μm absorption band of CO_2.

The analyzer was located in the container at the base of the tower. The instrument was operated in absolute mode by maintaining the reference cell at zero concentration by a soda-lime scrubber in a closed loop arrangement. The sample cell outlet was connected to a vacuum source with a hot-wire based flowmeter (Allborg Mass Flowmeter, model GFM-1700) placed in between the

vacuum and cell. The flowmeter voltage output was calibrated using a bubble flowmeter connected in series between the mass flowmeter and the vacuum source (see Figure 2.1).

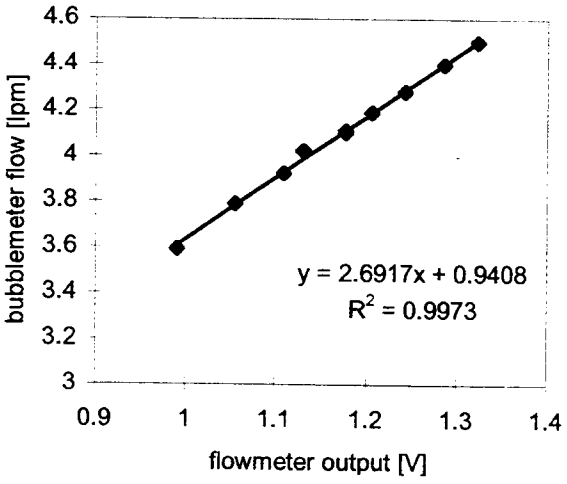

Figure 2.1 Mass flowmeter output calibration (Julian-day 266)

The Licor sample inlet was attached to a short sample tube with a two-way solenoid at the end. The solenoid was used to switch between a sample tube and an analyzer zero-offset check system.

One inlet of the solenoid was linked to a 12 m long high-density polyethylene tube with inner diameter of 3.175 mm. The end of the sample tube was co-located with a fast response temperature sensor 10 cm from the vertical transducer path of the ATI sonic head. The tube flow rate of 4 liters per minute was driven by a vacuum source at the outlet of the analyzer. This flow rate results in a transient time of 0.15 seconds in the analyzer sampling cell (V_{cell}=11.9 cm^3).

The gas analyzer was checked periodically for its CO_2-zero-concentration offset. Changes in the zero-offset occur due to temperature shifts or dirt entering the optical path of the measurement cells. The CO_2 zeroing system included a soda-lime scrubber canister ($V = 0.65\ dm^3$) and an AC switching box controlled by a personal computer with an analog output, and control port peripheral. The scrubber was connected to the second inlet of the solenoid at the analyzer inlet. The CO_2 zero check was software controlled; the solenoid connection to the zeroing tube/scrubber was switched on every 1740 s for a duration of 20 s (after 07/08/94 these were changed to 1730 and 30 seconds, respectively). The analog output provided a mode signal, which was logged on a 1 Hz basis. The signal was used to distinguish between operational and zero-offset-check periods. A mode signal of higher than 0.1 volt was regarded as analyzer zeroing time period, while no voltage output occurred when the analyzer sampled ambient air. To ensure a complete determination of the CO_2 zero check period and removal of zeroing data from the operational CO_2 concentration readings, the mode signal data were shifted forward in time by 5 seconds and ambient data were discarded for 10 seconds after the mode voltage dropped down to zero again.

Early in the experiment (Julian-days 223-242) the orientation of the scrubber canister was horizontal, which caused some air to bypass the soda lime granules. After turning on the CO_2 zero check, the air, that was resident in the scrubber during the last operational period and consequently carbon dioxide free, was ducted through the analyzer. As a result, a short zero concentration reading of about 3 seconds duration was recorded by the analyzer and afterward the output signal rose slowly due to the incomplete CO_2 removal in the ducted air (see Figure 2.2). The time duration of the short zero offset reading can be estimated by the volume of carbon dioxide free air ($V \approx 0.2\ dm^3$) drawn with a flow rate of 4 liter per minute.

On Julian-day 243 at 18:45 the orientation of the scrubber was changed to vertical to ensure air flow through the soda-lime granules. This resulted in a

complete removal of the carbon dioxide over the whole time air was ducted through the scrubbing canister (see Figure 2.3). This orientation was maintained until the end of the experiment on Julian-day 265.

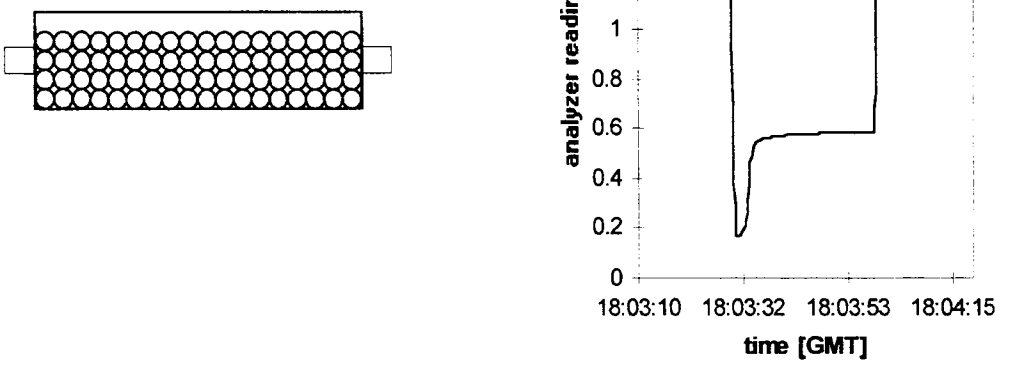

Figure 2.2 CO_2 analyzer zero reading for horizontal scrubber orientation at Julian-day 243

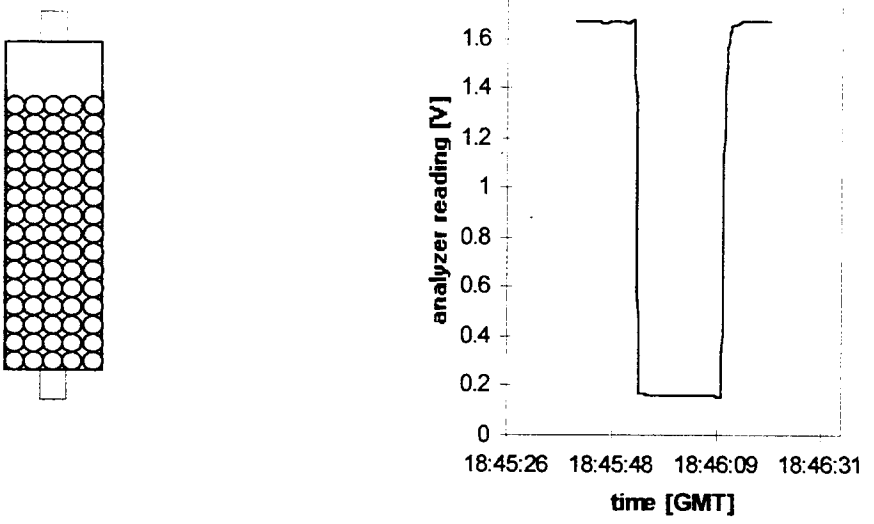

Figure 2.3 CO_2 analyzer zero reading for vertical scrubber orientation at Julian-day 243

2.3.2 Sonic Anemometer

The sonic anemometer measures wind speed (u, v, w) along three orthogonal axes (x, y, z) and virtual temperature (T_v) derived from the w-component. The instrument works on the principle that the speed of sound increases if air moves in the same direction as a sound pulse. Hence the difference in transit time of forward and backward sound pulses between two ultrasonic transducers can be used to derive wind speed. Let t_1 and t_2 be the forward and backward transit times for a sound pulse of speed C and transducer separation L. The transit times with an air flow in the direction of the transducer path are given by (Applied Technologies, 1993; Gill Instruments, 1992)

$$t_1 = \frac{L}{C + w} \tag{10}$$

$$t_2 = \frac{L}{C - w} \tag{11}$$

where w is the wind speed in the direction of the sound path of length L, and C is the velocity of sound.

Wind speed parallel to the sound path (w) and the speed of sound (C) are derivable from the forward and backward transit times between the z-transducer path as

$$C = \frac{L}{2} * \left(\frac{1}{t_1} + \frac{1}{t_2}\right) \tag{12}$$

$$w = \frac{L}{2} * \left(\frac{1}{t_1} - \frac{1}{t_2}\right) \tag{13}$$

and the virtual temperature is given by the assumption of a sound wave propagating in an ideal gas, where the speed of sound is a function of temperature (Applied Technologies, 1993)

$$C^2 = \frac{\gamma R T_v}{M} \tag{14}$$

$$T_v = \frac{C^2 M}{\gamma R} \tag{15}$$

where $\gamma = C_p/C_v$ is the ratio of the specific heats of air at constant pressure and constant volume, M is the molecular weight of air, R is the universal gas constant, and T_v is the virtual temperature, the temperature of dry air having the same density as moist air at the same pressure.

2.3.3 Platinum Resistance Temperature Probe

The fast response temperature sensor operates on the principle that the electrical resistance of materials depends on temperature. The resistance of many metals is a nearly linear function of temperature. The most commonly used metal is high purity platinum wire, which shows a excellent linearity between temperature and resistance. A small current is sent through the wire, which is

exposed to the environment and the voltage drop across the sensor is measured. The resistance at temperature T is given by

$$R_T = R_o [\, 1 + A\,(T - T_o)] \qquad (16)$$

where R_T is calculated from the voltage drop and the supplied current, R_o is a reference resistance determined for a temperature T_o, and A is a calibration constant.

2.3.4 Krypton Hygrometer

The Krypton hygrometer measures the atmospheric water vapor concentration based on the attenuation of UV radiation in an open-path sensing volume. The UV radiation is produced by a krypton glow tube, which emits radiation at 116.49 and 123.58 nm. Water vapor absorbs strongly around the Lyman-α line (121.56 nm), absorption of other gases at this wavelength is weak. The water vapor concentration (ρ_W) can be determined from the total received intensity of the two bands (Campbell and Tanner,1985), after attenuation due to the water vapor content in the volume between the source and detector,

$$\rho_W = \frac{\ln\left(J/J_T\right)}{L k_W} - \frac{k_{O2}}{k_W}\frac{c P M_O}{R T} \qquad (17)$$

where J and J_T are the received and transmitted total intensity of both bands, L is the gap length between source and detector, k_W and k_{O2} are the extinction coefficients of water vapor and oxygen (band 2 only), c is the volume fraction of oxygen in air (0.21), P is the atmospheric pressure, M_O is the molecular weight of oxygen, R is the gas constant, and T is the temperature.

2.4 Data Acquisition System

The ASTER data acquisition system setup began August 1, 1994. The system was operational by Julian-day 220 (August, 8th) and ran continuously until Julian-day 265 (September, 23rd) 1994.

The deployed instruments were connected to automatic data acquisition modules (ADAM), which were connected to a base computer (UNIX workstation). The ADAM's are real-time operational units capable of gathering and processing digital, analog or serial data from integrated or intelligent sensors.

The base computer reads the processed data from the ADAM's, calculates and displays summary information and archives the raw data. Each day at 24:00 hours GMT, 17:00 pacific daylight savings time (PDT), the data were backed up onto 8 mm storage tapes. The calculated summary information included mean and covariance computations for 5 minute intervals for certain specified signal combinations. The results of those calculations were stored as "covar-files" on the UNIX system.

After the experiment the data (raw data files and covar-files) were transferred to the NCAR computer system in Boulder, Colorado. The data are accessible by remote login at atd.ucar.edu. A standard statistical analytic programming language (Splus) was used to analyze the raw- and covar-data.

2.5 Eddy Correlation

The eddy correlation technique is based on measurement of turbulent wind variations and associated fluctuations of scalars, such as temperature, water vapor content, or gas concentrations. The measured turbulence consists of eddies (swirls of air motion superimposed on the mean wind) with various sizes, directions and time scales. The transport of a scalar quantity by those eddies is the so-called "eddy flux" or "turbulent flux". The eddy flux $\overline{w'C'}$ in the

vertical wind direction (w) of a scalar (C) can be calculated with fast response sample data as

$$\overline{w'C'} \equiv \frac{1}{N}\sum (w - \bar{w})(C - \bar{C}) \qquad (18)$$

where w' or C' are deviations of individual samples (w) or (C) from the mean values ($\bar{w}$)or ($\bar{C}$) (overbars denote a time average) in the sampled time period consisting of N data points. Thus the eddy flux of a scalar is given by the covariance of that scalar with the wind speed in the direction of interest.

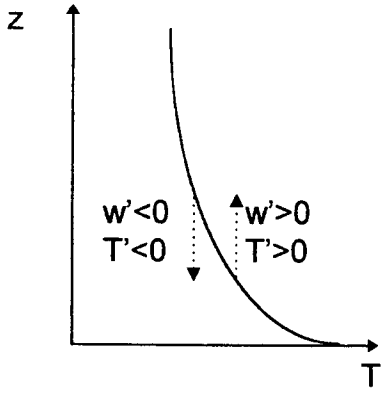

Figure 2.4 Idealized eddy mixing process in the case of temperature (T) decrease with height (z)

In the case of an idealized eddy mixing process in an unstable environment (hot summer day over land where temperature decreases with height z), eddies mix warmer air up (T'>0, w'>0) and colder air down (T'<0, w'<0) (see Figure 2.4). The net eddy sensible heat flux $\overline{w'T'}$ is positive, since in both cases the product w'T' is positive, corresponding to an upward heat flux.

The horizontal flux terms are computed in an analogous manner. The streamwise horizontal flux is $\overline{u'C'}$ and the crosswind horizontal component is $\overline{v'C'}$. Eddy fluxes can be calculated for various types of scalars:

$\overline{w'C'_{CO2}}$	vertical eddy CO_2 flux
$\overline{w'T'}$	vertical eddy sensible heat flux
$\overline{u'w'}$	vertical eddy flux of horizontal momentum

2.6 Data Preprocessing

Fast response data time series generally are "cleaned" before computing covariances in eddy correlation. The time series often are processed by despiking, rotation into a different coordinate system, and detrending with high-pass filtering (Baldocchi et al., 1988; McMillen, 1988; Stull, 1988). Despiking removes anomalous large or small values (Spikes) caused by non-meteorological events (Hojstrup, 1993). Rotation allows the interpretation of a flux oriented normal to the mean streamwise wind. Detrending with high-pass filtering eliminates non stationary trends within the averaging time period.

The sonic anemometer data were despiked according to the procedure of Hojstrup (1993), which identifies anomalous data spikes caused by electronic measurement errors, a blocked path between the transducers, or accumulated water on the transducer surface. The spike removal algorithm determines an unusual measurement by calculating a prediction variance based on the difference between the measured wind speed and a predicted value, which itself is based on the serial correlation in the wind speed component. The prediction variance for a data point is compared to a pooled variance for a "memory" consisting of the (10^2 to 10^3) most recently acquired data points from the same variable. When the prediction variance exceeds the memory based variance by more than 6 times its magnitude, the data point is identified as spike. A detected spike is replaced by its predicted value and the data point is flagged as a spike. If the spike occurrence in the wind speed time series used for a flux calculation exceeds one percent, the calculated flux is not used for further analysis.

Due to imperfect sensor alignment and non-homogenous terrain, coordinate rotations are necessary to determine the surface flux normal to the streamlines (Baldocchi et al., 1988). The rotation scheme transforms the three measured mean wind components from an orientation aligned with the instrument axes to a new orientation, where the x-component $\bar{u}$ is aligned into the mean wind, and consequently the rotated mean vertical $\bar{w}$ and horizontal

crosswind $\bar{v}$ are zero over the flux time period. The azimuthal (η) and zenith (θ) rotation angles are calculated from the three orthogonal mean wind components $\bar{u}_{unrot}$, $\bar{v}_{unrot}$, and $\bar{w}_{unrot}$ (means over the flux time period calculated before rotation) according to

$$\eta = \tan^{-1} \frac{\bar{v}_{unrot}}{\bar{u}_{unrot}} \tag{19}$$

$$\theta = \tan^{-1} \frac{\bar{w}_{unrot}}{(\bar{u}_{unrot}^2 + \bar{v}_{unrot}^2)^{0.5}} \tag{20}$$

and the magnitude of the instantaneous, rotated wind components (u_{rot}, v_{rot}, w_{rot}) are given by transformation of the unrotated data samples u_{unrot}, v_{unrot}, w_{unrot} according to

$$u_{rot} = u_{unrot} \cos(\eta) \cos(\theta) + v_{unrot} \sin(\eta) \cos(\theta) + w_{unrot} \sin(\theta) \tag{21}$$

$$v_{rot} = -u_{unrot} \sin(\eta) + v_{unrot} \cos(\eta) \tag{22}$$

$$w_{rot} = -u_{unrot} \cos(\eta) \sin(\theta) - v_{unrot} \sin(\eta) \sin(\theta) + w_{unrot} \cos(\theta) \tag{23}$$

The detrending procedure uses an approximation to a running mean as a high-pass filter to remove trends with wavelengths longer than about one-third to one-fifth of the time series length and retain enough complete cycles of shorter wavelength for significant statistical averaging (Stull, 1988). Detrending was undertaken with a running-mean high-pass filter following McMillen (1988), which is given by

$$y_i = \alpha y_{i-1} + (1-\alpha) x_i \tag{24}$$

where x_i is a sample taken at time t_i, y_i is the trend of the data series at t_i, and α is a filter parameter defined by

$$\alpha = e^{-\frac{1}{f\tau}} \tag{25}$$

where f is the sample frequency, τ is the time constant of the filter.

The deviations from the running mean data series are then calculated with

$$x_i' = x_i - y_i \qquad (26)$$

A 200 second filter time constant was used in the detrending procedure. A analysis of field data of a previous field experiment at the same location showed that the value of 200 s retained virtually all of the scalar fluxes while resulting in a physically realistic downward momentum flux (Vong and Kowalski, 1995).

2.7 Data Analysis

The eddy flux computations for latent (LE) and sensible (H) heat flux, and carbon dioxide flux (F_{CO2}) were performed for the period from Julian-day 223 to 262. Fluxes were calculated for ~28 minute intervals, as determined by the frequency of the gas analyzer zero offset checks. For each eddy flux calculation the wind speed data were despiked, rotated and detrended. The scalar data were detrended with the same filter constant of 200 seconds. Covariance eddy fluxes were computed from both the detrended and non-detrended sample data. The scalar instrument and sonic anemometer combination for each calculated eddy flux are shown in Table 2.1.

Table 2.1 Calculated eddy flux, instruments and tower Location

Surface flux	**Scalar instrument**	**Sonic**	**Location**
F_{CO2} ATI	Licor CO_2	ATI	10 m Walk
F_{CO2} SOLENT	Licor CO_2	SOLENT	10 m Walk
H ATI	Fast temperature	ATI	10 m Walk
LE ATI15	Krypton hygrometer	ATI	15 m Flux

Water vapor pressure deficit (VPD) was calculated with the assumption of well coupled leaves to the surrounding air (leaf temperature equals air temperature) according to

$$VPD = e_s(T_{air}) \cdot \left(1 - \frac{RH}{100}\right) \quad (27)$$

where e_s (T_{air}) is the saturation water vapor pressure at air temperature and RH is the relative humidity of the air.

Wind attack angle (α_{attack}) to the horizontal is calculated according to

$$\alpha_{attack} = \theta + \alpha_{Tilt} \quad (28)$$

where θ is the vertical rotation angle of the sonic wind speed data, and a_{Tilt} is the tilt angle of the x-axis of the sonic anemometer into the horizontal plane. A positive attack angle means wind is attacking upward from below the horizontal plane. The tilt angle of the ATI sonic and the Solent sonic to the horizontal boom was measured to 10° and 0°, respectively.

Wind direction (η_{wind}) in the horizontal plane is calculated according to

$$\eta_{wind} = \eta + \eta_{boom} \quad (29)$$

from the azimuthal rotation angle (η) and the azimuthal orientation (η_{boom}) of the sonic x-axis, which was aligned with the rotating boom. A direction of 0°, 90°, 180°, or 270° denotes wind coming from the North, East, South, or West, respectively.

The friction velocity u*, used as a measure of the strength of the turbulence, was calculated from the downward momentum flux $\overline{u'w'}$ according to

$$u^* = (-\overline{u'w'})^{1/2} \quad (30)$$

2.8 Carbon Dioxide Flux

The net carbon dioxide eddy flux was calculated from the covariance of the CO_2 analyzer output and the sonic wind speed component normal to the streamline. The CO_2 data were shifted forward in time by 1.4 s to compensate for the time delay introduced by the sampling technique (12 m long sample tube). The time delay of the CO_2 signal to the wind speed data was measured by blocking the sonic transducers in front of the sample tube inlet with a carbon-dioxide-filled balloon. The balloon was pinched and the delay determined from the time trace of w and CO_2 producing an estimate of 1.4 seconds for the time lag. This time delay agreed with calculated time lagged cross-correlation of the vertical wind component and fast temperature with the CO_2 signal. Further, the delay agrees well with a flow rate of 4 liters per minute through the 12 m long sample tube with diameter 3.175 mm, which results in 1.35 seconds transient time in the tube.

The carbon dioxide signal was sampled at 20 Hz, whereas the sampling rate was 10 Hz for the ATI sonic anemometer and 21 Hz for the Solent sonic. For the eddy flux calculation the data streams from the sonic and gas analyzer were synchronized to the frequency of 10 Hz.

The time duration for the flux calculation was defined by the CO_2 analyzer operational periods, which were fixed in between two analyzer zero offset checks. The zero checks were performed on a ~28 minute basis during the entire experiment.

The CO_2 flux was scaled under the assumption, that the daily mean analyzer signal voltage ($V_{CO2.day}$) is equivalent to 353±10 $\mu l\ l^{-1}$ of atmospheric CO_2. This ambient carbon dioxide concentration was determined by calibration checks with a standard span gas of 378 $\mu l\ l^{-1}$ (Scott Specialty Gases, Inc. Acublend Master Gas carbon dioxide in air mixture N_2/O_2; nominal analytic accuracy of 1%). During calibration checks, a plastic bag was attached to the sampling tube on top of the tower and the calibration gas was fed into an open T

junction at the inlet of the bag. The inflow into the T junction was maintained slightly above the analyzer flowrate to keep ambient air from entering the bag. The bag was kept one-third to two-third filled to insure consistent pressure conditions with the ambient environment. The analyzer voltage output (V_{cal}) and analyzer zero signals (V_{zero}) were recorded. The ambient concentration was calculated from the ambient voltage signal ($V_{ambient}$) with a linear analyzer response assumption, according to

$$C_{ambient} = \frac{378\ \mu l\ l^{-1}}{V_{cal} - V_{zero}} * (V_{ambient} - V_{zero}) \qquad (31)$$

The conversion of the CO_2 eddy flux from the calculated covariance $\overline{w'V'_{CO2}}$ in units of [m s^{-1} V] to a molar concentration flux F_{CO2} in units [µmol m^{-2} s^{-1}] for standard atmosphere conditions is given by

$$F_{CO2} = \frac{C_{ambient}}{V_{CO2.day}} \cdot \frac{1mol}{22.4E\text{-}3m^3} \cdot \frac{P_{baro}}{1013hPa} \cdot \frac{273K}{T_{air}} \cdot \overline{w'V'_{CO2}} \qquad (32)$$

$$= A_0 \cdot \overline{w'V'_{CO2}} \qquad (33)$$

with A_0 is a calibration coefficient depending on the ambient CO_2 concentration $C_{ambient}$ of 353±10 µl l^{-1}, the analyzer signal output $V_{CO2.day}$ averaged over the entire day, and the mean air temperature T_{air} and atmospheric pressure P_{baro} over the flux time period.

2.9 CO_2 Flux Uncertainties

An error in the CO_2 flux arises from any error in the calculated covariance term $\overline{w'V'_{CO2}}$ and any error in the calibration coefficient.

The error introduced in the covariance term $\overline{w'V'_{CO2}}$ mainly arises from density fluctuations in the sampled air (Webb et al., 1980; Leuning and King, 1992; Leuning and Moncrieff, 1990), and from damping-out of high frequency

variations of the carbon dioxide concentration in the sampling tube (Leuning and Moncrieff, 1990; Leuning and King, 1992).

Webb et al. (1990) showed that corrections must be made for the influence of heat and water vapor fluxes on density fluctuations in carbon dioxide concentration. The correction term associated with sensible heat flux plays a minor role for a closed-path gas analyzer, since the sampled air for updrafts and downdrafts adjusts to a common temperature during the flow through the sampling tube and into the measurement unit (Leuning and Moncrieff, 1990; Leuning and King, 1992). The major part of the correction is caused by the water vapor fluctuations that are associated with a latent heat flux. Leuning and Moncrieff (1990) obtained the following expression for the CO_2 flux correction term for a closed path analyzer system

$$\delta F_{CO2} = \left(\mu \frac{\rho_c}{\rho_a} - \chi\right)\left(\overline{w'\rho'_{H2O}} + \frac{\rho_{h2o}}{T}\overline{w'T'}\right) \tag{34}$$

$$= \left(\mu \frac{\rho_c}{\rho_a} - \chi\right)\left(\frac{LE}{\lambda} + \frac{\rho_{h2o}}{\rho_a}\frac{H}{C_p T}\right) \tag{35}$$

where χ is a CO_2 analyzer water vapor sensitivity factor, $\mu = m_a/m_v$ is the ratio of the molecular weights of dry air and water, ρ_c, ρ_a, and ρ_{h2o} are mean density of carbon dioxide, dry air, and water vapor, T is the mean air temperature in K, λ is the latent heat of evaporation, C_p is the specific heat of air at constant pressure, LE and H are latent and sensible heat flux in W m^{-2}. With representative values T = 288 K, $\rho_c/\rho_a = 5.39 \times 10^{-4}$ at the mean CO_2 content of 353 $\mu l\ l^{-1}$, $\rho_{h2o}/\rho_a = 6.28 \times 10^{-3}$, and $\chi = 3.17 \times 10^{-4}$ for a LICOR LI-6251 gas analyzer (Leuning and King, 1992), the correction term reduces to

$$\delta F_{CO2} = 5.5 \times 10^{-4}\ (4.1 \times 10^{-4}\ g\ J^{-1}\ LE + 2.1 \times 10^{-8}\ g\ J^{-1}\ H) \tag{36}$$

The correction term δF_{CO2} for periods with high CO_2 flux values (midday with high input of net radiation of more than 300 W m^{-2}) can be estimated from the upward sensible and latent heat fluxes, which were in the range of 150 to 250 W m^{-2}. The correction δF_{CO2} under these conditions computes to ~+0.045

mg-CO_2 m^{-2} s^{-1} (≈1 μmol m^{-2} s^{-1}). The Webb correction term is ~10 percent of typical midday CO_2 fluxes of -8 to -14 μmol m^{-2} s^{-1}.

For time periods with smaller CO_2 fluxes due to reduced input of net radiation (early morning or clouds concealing the sun), the sensible and latent heat fluxes and the correction term generally would be smaller. Nevertheless, the correction can result in a sign change of the carbon dioxide flux, for periods where the correction term exceeds the measured CO_2 flux.

Leuning and King (1992) showed that a closed path CO_2 analyzer (Licor, model LI-6251) underestimates the flux by an average of 16 percent relative to an open path analyzer (Advanced Systems Inc., model E009). The flux measured by a closed path analyzer at frequencies greater than 0.1 Hz was lower than for the open-path analyzer, because high frequency density fluctuations were damped by the sampling tube.

The relative error in the calibration coefficient A_0 can be derived from

$$\frac{\delta(A_0)}{A_0} = \frac{\delta(C_{ambient})}{C_{ambient}} + \frac{\delta(P_{baro})}{P_{baro}} + \frac{\delta(T_{air})}{T_{air}} \qquad (37)$$

with typically values of $C_{ambient}$ = 353±10 μl l^{-1}, P_{baro} = 960±5 hPa, and T_{air} = 288±2 K, the relative error computes to

$$\frac{\delta(A_0)}{A_0} \approx \frac{10\ \mu l\ l^{-1}}{353\ \mu l\ l^{-1}} + \frac{5\ hPa}{960\ hPa} + \frac{2\ K}{288\ K} \approx 4\ \% \qquad (38)$$

Hence, for periods with high input of net radiation the flux loss due to damping in the sample tube and the Webb correction are comparable in magnitude, but opposite in sign. A relative error in the CO_2 flux for those time periods would be about 15 percent including the possible small relative error in the calibration coefficient. The absolute error of typically high fluxes of -8 to -14 μmol m^{-2} s^{-1} is ~1 to 2 μmol m^{-2} s^{-1}.

Due to the lack of reliable latent heat fluxes for parts of the experiment duration (Kr Hygrometer failure due to the frequent interception of cloud water)

an individual correction for density fluctuations was not performed. Instead it was assumed, that the absolute error introduced due to the dampening out of high frequency fluctuations in the sampling tube, the Webb correction, and any error in the calibration coefficient are less than ±2 μmol m^{-2} s^{-1}. The error of 2 μmol m^{-2} s^{-1} was derived from the relative error of ~15 percent under conditions of high input of net radiation.

2.10 Energy Balance

A state of energy balance for the atmosphere-surface system occurs when the energy put into the system is equal to the energy lost out of the system over a specified time frame. The major contributor of incoming energy for the atmosphere-surface layer is solar radiation, where the net input of radiation-energy is determined by the difference in incoming and outgoing short and long wave radiation:

$$R_n = (R_{s.in} - R_{s.out}) + (R_{l.in} - R_{l.out}) \qquad (39)$$

where R_n denotes net radiation, R_s and R_l are the short and long wave radiation components.

During the day, net radiation absorbed by the surface is returned to the atmosphere primarily by conduction and turbulent exchange. A small portion is typically stored as internal energy (temperature raise of the system) or biochemical energy (photosynthesis by plants). During daytime, the warmer surface transports heat by conduction and evaporation into the lowest atmosphere layer, where turbulent transport dominates. A loss of energy for the system results due to sensible and latent heat fluxes being directed away from the surface. Some part of the heat is conducted into the ground, which results in a ground heat flux.

At nighttime, energy exchange in the atmosphere-surface system is generally smaller, because of the missing energy input by short wave radiation.

Atmospheric conditions (e.g. the difference in air-surface temperature, cloud cover, and evaporation or condensation of water) control the magnitude and direction of net radiation, sensible and latent heat exchange, ground heat flux, and changes in energy storage.

The overall energy balance for the atmospheric surface layer can be written as

$$R_n - S = H + LE + G \tag{40}$$

where R_n is incoming net radiation, S is energy storage, H is sensible heat flux, LE is latent heat flux, and G is ground heat flux. The common sign convention for net radiation is positive value for energy directed towards the system. Heat fluxes are by convention positive or negative if they are directed away from or towards the system, respectively. Increase of stored energy in the system mass is positive, and release is negative.

The soil contribution (G and S) to the energy budget was determined from five minute mean heat flux plate measurement values G_{soil} and a soil temperature storage term calculated as the time derivative of the soil temperature T_{soil} times a storage capacity factor C_{soil} and soil layer depth D, where the soil temperature is a weighted mean temperature of the measurements at different depths (1, 3, 5, and 7 cm) in the upper soil layer:

$$G + S = G_{soil} + C_{soil} D \frac{dT_{soil}}{dt} \tag{41}$$

$$T_{soil} = \frac{1}{8} (T_{1cm} + 3\,T_{3cm} + 3\,T_{5cm} + T_{7cm}) \tag{42}$$

Sensible and latent heat flux (H and LE) are calculated from measured eddy fluxes as

$$H = C_p \rho_a \overline{w'T'} \tag{43}$$

$$LE = \lambda \overline{w'\rho'_{H2O}} \tag{44}$$

where C_p is the specific heat of air, ρ_a is the air density, λ is the latent heat of evaporation, and $\overline{w'T'}$ is the eddy heat flux and $\overline{w'\rho'_{H2O}}$ is the eddy moisture flux normal to the wind streamlines.

2.11 Data Screening

A screening (Standard Screening) of the derived data was performed to ensure minimal influence of measurement problems due to possible flow distortion, anomalous spikes in the data, or measurement interruptions.

The wind direction was limited to the sector 180° to 270° (South to West) to decrease possible flow distortion due to more complex terrain outside the sector (Federal Aviation Administration to the North, Makah Peak to the South East), and wind sheltering due to the instrument towers and containers located at the North, East, and South-East side of the hilltop.

The number of spikes in a 28 minute flux time period, flagged by the despiker routine, was limited to a reasonably small number ($f < 1$ %) following Vong and Kowalski (1995).

Data were discarded for time periods of measurement interruptions (e.g. instrument maintenance or boom rotations into the mean wind).

The measurements of carbon dioxide flux for the Julian-days 223 to 262 resulted in a total of 1959 twenty-eight-minute periods available for further analysis. The derived CO_2 flux for a time period was screened out, if any of the above mentioned conditions was met for that time period. This screening is going to be referred to as the Standard Screening. The number of time periods retained after performing the Standard Screening and screening for various analysis specific conditions (e.g. daylight or nighttime) is shown in Table 2.2.

Table 2.2 Data screening summary

Screening for	**retained time periods**	**retained in %**
Wind direction in 180° to 270°	1073	55 % of 1959
Number of spikes in sonic data < 1 %	1739	89 % of 1959
No maintenance or boom rotation	1615	82 % of 1959
Standard Screening: - Wind direction in 180° to 270° - Number of spikes in sonic data < 1% - No maintenance or boom rotation	742	38 % of 1959
Daylight (IPAR > 5 μmol m^{-2} s^{-1}) AND Standard Screening	458	62 % of 742
Nighttime (IPAR < 5 μmol m^{-2} s^{-1}) AND Standard Screening	284	38 % of 742
Daylight (IPAR > 5 μmol m^{-2} s^{-1}) AND no surface cloud (LWC < 0.01 g m^{-3}) AND Standard Screening	232	31 % of 742 51 % of 458
Nighttime (IPAR < 5 μmol m^{-2} s^{-1}) AND no surface cloud (LWC < 0.01 g m^{-3}) AND Standard Screening	48	6 % of 742 17 % of 284

3. Results

3.1 Forest

The major tree species in the 100 m long transect down the South-West slope are Pacific Silver Fir with 79% of total tree leaf dry biomass (LBM) and Western Hemlock with 18%. The average age of the Fir and Hemlock trees close to the hill top was 25 years in 1994. Mean leaf area index (LAI), leaf dry biomass (LBM), basal area (BA), and average height of the major tree species in the transect are shown in Table 3.1. The distributions of LAI, LBM, BA, and tree height over the whole transect are shown in Figure 3.1. The understory consists mostly of Salal (~40 percent of absolute shrub cover).

Table 3.1 Mean data of forest transect plots (n = 10), Abam = *A. amabilis*, Tshe = *T. heterophylla*, Thpl = *T. plicata* (no *T. plicata* data on 8 of the 10 plots. Means are for all 10 plots.)

	Abam	**Tshe**	**Thpl**	**total**
LAI	5.0	1.9	0.1	7.0
LBM ($g\ m^{-2}$)	873.9	216.0	23.0	1112.9
BA ($m^2\ ha^{-1}$)	14.1	4.9	0.3	19.3
average height (m)	6.7	6.4	1.0	NA

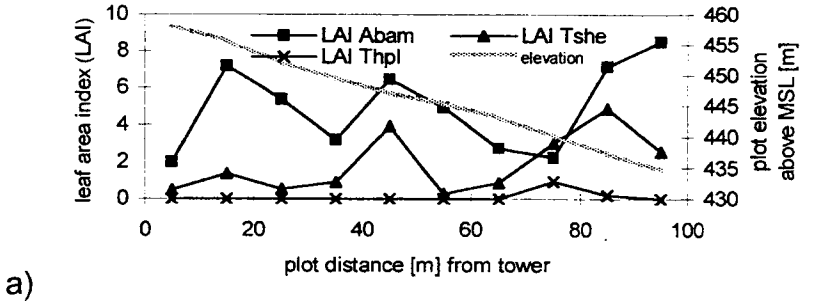

a)

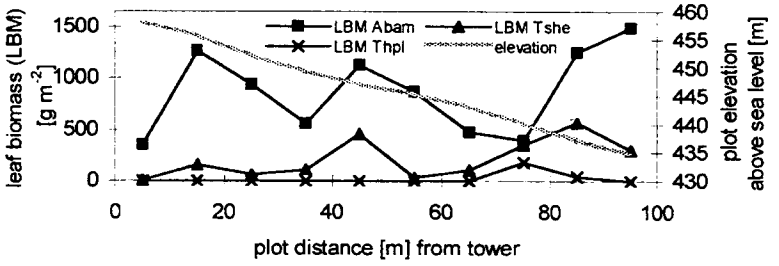

b)

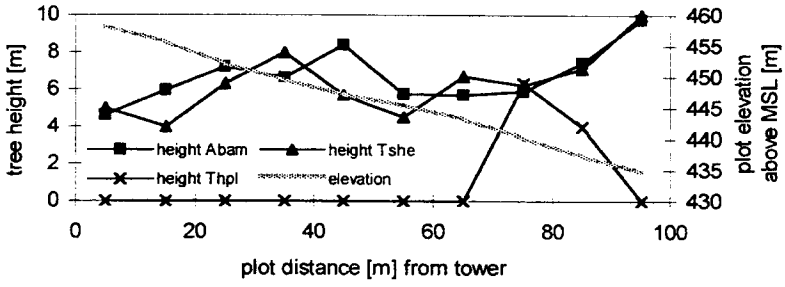

c)

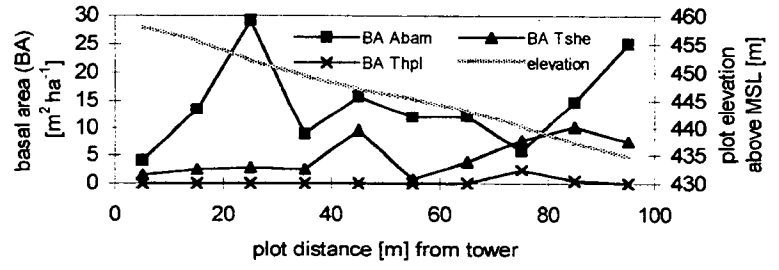

d)

Figure 3.1 Transect a) leaf area index (LAI), b) leaf biomass (LBM), c) average tree height, and d) basal area (BA) for *A. amabilis*, *T. heterophylla*, and *T. plicata* with transect plot elevation above mean sea level (MSL) superimposed

3.2 Carbon Dioxide Analyzer Reading

The LICOR CO_2 analyzer was operational from Julian-days 223 to 266. The output of the analyzer was sampled at 20 Hz and recorded uncalibrated as a raw voltage signal.

The analyzer net CO_2 concentration output expressed in volts (analyzer output minus the last analyzer zero offset) (see Figure 3.2) stayed consistent over periods of a few days. Two effects on the analyzer output and zero offset were flowrate adjustments and contamination of the analyzer optics due to dirt entering the measurement cell. The zero offset generally showed a slow increase from the beginning of the experiment, which suggests a gradual increase of non-carbon-dioxide absorption (e.g. - that due to particles) in the optical path . On Julian-day 249 a large offset jump of 0.5 volts in both the analyzers operational and zero reading occurred (Figure 3.2), probably due to cloud water contaminating the analyzer optics.

The low CO_2 output voltages at the beginning of the experiment (days 222 to 224) are due to an inoperative jumper for the zero mode signal at the A/D board in the automatic data acquisition module. After 11:35 PDT on Julian-day 224 the jumper was set correctly and the CO_2 analyzer zero check periods were indicated accurately. The spikes during Julian-days 238, 240, 242, 249, and 259 are due to instrument maintenance periods.

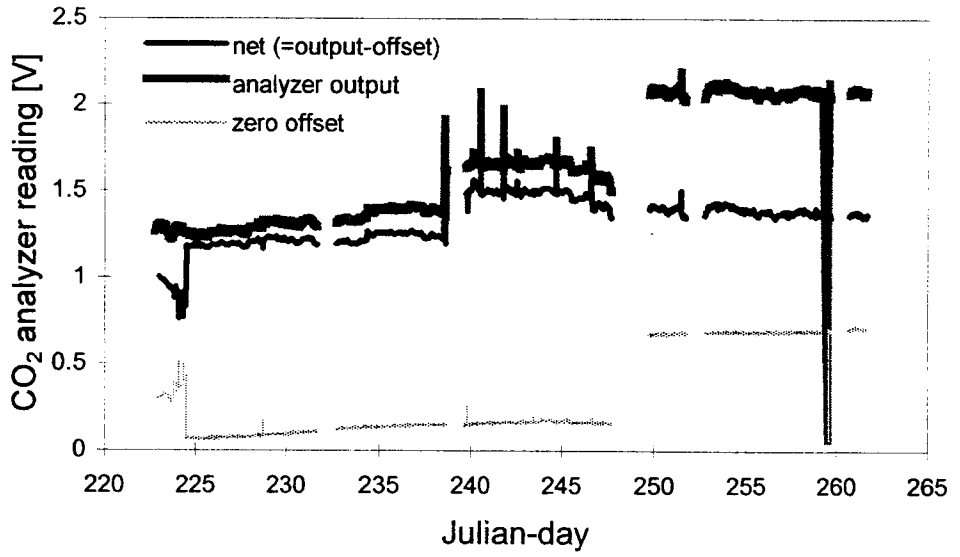

Figure 3.2 CO_2 analyzer mean output and zero reading

The ambient atmospheric carbon dioxide concentration $C_{ambient}$ was estimated to 353±10 $\mu l\ l^{-1}$ through the use of a calibration gas consisting of 378 $\mu l\ l^{-1}$ CO_2 mixed in air. Calibration checks were performed on Julian-days 242, 244, 254, and 259. The estimated ambient carbon dioxide concentrations are shown in Table 3.2. The mean concentration agreed very well with flask trace gas measurement undertaken by the National Oceanic and Atmospheric Administration at locations in Oregon (Cape Meares, 45° 29' N, 124° 0' W) and Alaska (Cold Bay, 55° 12' N, 162 43' W), which showed mean concentrations of 350 $\mu l\ l^{-1}$ (July) to 355 $\mu l\ l^{-1}$ (September) during the summer periods of previous years (Conway et al., 1994).

Table 3.2 Carbon dioxide ambient concentration ($C_{ambient}$), V_{cal} = analyzer output [V] sampling calibration gas (378 $\mu l\ l^{-1}$), V_{zero} = analyzer zero offset [V], $V_{ambient}$ = analyzer output [V] sampling ambient air

Julian-day	V_{cal}	V_{zero}	$V_{ambient}$	$C_{ambient}$
242	1.75	0.16	1.65	354
244	1.78	0.166	1.65	348
254	2.18	0.686	2.08	353
259	2.20	0.697	2.106	354

The flowrate through the LICOR was maintained at 4 liters per minute, and was monitored with a mass flowmeter. The CO_2 reading of the gas analyzer was dependent on the flowrate through the sample cell. The analyzer output had a linear response to changes in the flowrate, which was determined by introducing step changes in the flowrate and monitoring the CO_2 instrument response. Figure 3.3 shows the response of the CO_2 analyzer to step changes manually introduced at around 23:40 GMT on Julian-day 244. The flowrate through the instrument showed minor long term variations, but these apparently did not affect the calculated carbon dioxide flux, because the detrended and non-detrended covariance calculations are quite similar (Appendix A). As expected, the long term trends are not correlated to the vertical wind speed variations. Minor step changes in the analyzer output after CO_2 zero check periods were caused by small flowrate jumps. Those changes do not influence the calculations, because fluxes are computed for the time from one zero-check to the next one, and constant offsets in the signals are removed by the eddy correlation technique.

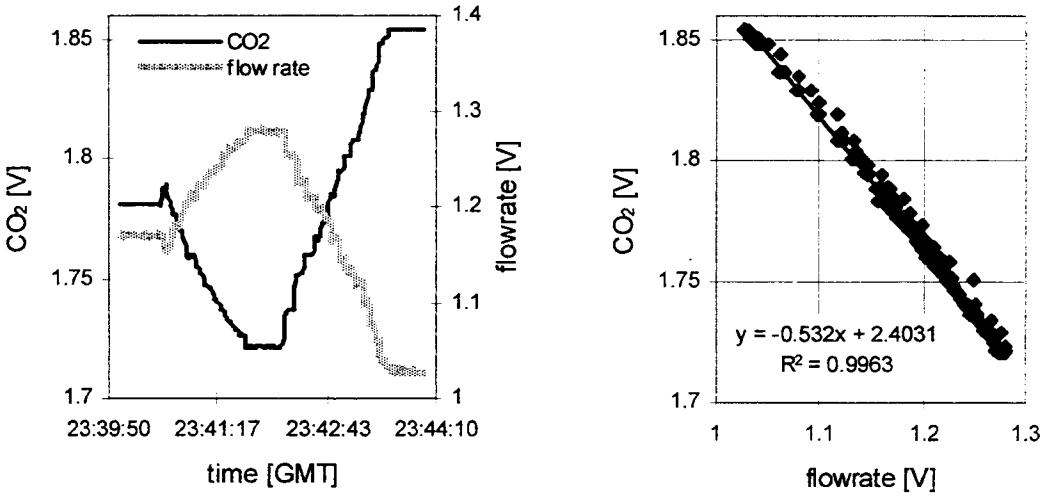

Figure 3.3 IRGA LI-6251 response to manually introduced flowrate changes

3.3 Daily CO_2 Flux Time Trace

CO_2 fluxes were calculated for 40 days from Julian days 223 to 262. The flux calculations for the days 263 to 266 were omitted because the wind direction stayed mostly outside the defined sector of 180° to 270°. The daily net carbon flux can be categorized into three distinctive incoming radiation classes: high midday incident PAR above 1200 μmol m^{-2} s^{-1}, mid-range midday incident PAR between 600 to 1200 μmol m^{-2} s^{-1}, low incident PAR less than 600 μmol m^{-2} s^{-1}.

The CO_2 flux time traces show a clear diurnal pattern for days with a sufficient amount of incoming radiation. Net uptake (negative CO_2 flux) of carbon dioxide occurred during daylight hours with a substantial input of photosynthetically active radiation. Release of CO_2 (positive flux) occurred at night due to plant and soil respiration. Typically the net flux was zero at one or two hours after sunrise, representing a balance between upward respiratory flux and downward flux from photosynthesis. The light compensation point, where the respiration rate equals the photosynthetic rate, was between 150 and 250 μmol m^{-2} s^{-1} of incident PAR.

Clouds occurred frequently for winds in the sector of 180° to 270°. For a total of 742 day and night 28-minute flux periods (retained after applying the Standard Screening) 62 percent had a LWC > 0.01 g m^{-3}, which is an indicator for surface cloud at the site. The difference in downward-long-wave-radiation temperature and air temperature (T_{sky} - T_{air}) indicates cloud cover overhead, because clouds emit long wave radiation in a first approximation as black bodies. Days with surface clouds or low level cloud cover overhead had a difference "T_{sky} -T_{air}" that was greater than -2.5 K. For those days, the daily maximum incident PAR measured at the surface was reduced compared to periods without cloud or thin and patchy cloud (T_{sky}-T_{air} < -7.5 K) (see Figure 3.4). This decrease is probably related to multiple scattering, reflection, and absorption of radiation by the cloud droplets. The reduced input of radiation results in lower photosynthetic activity and is observed as generally lower maximum carbon flux values during those cloud conditions (see Figure 3.5).

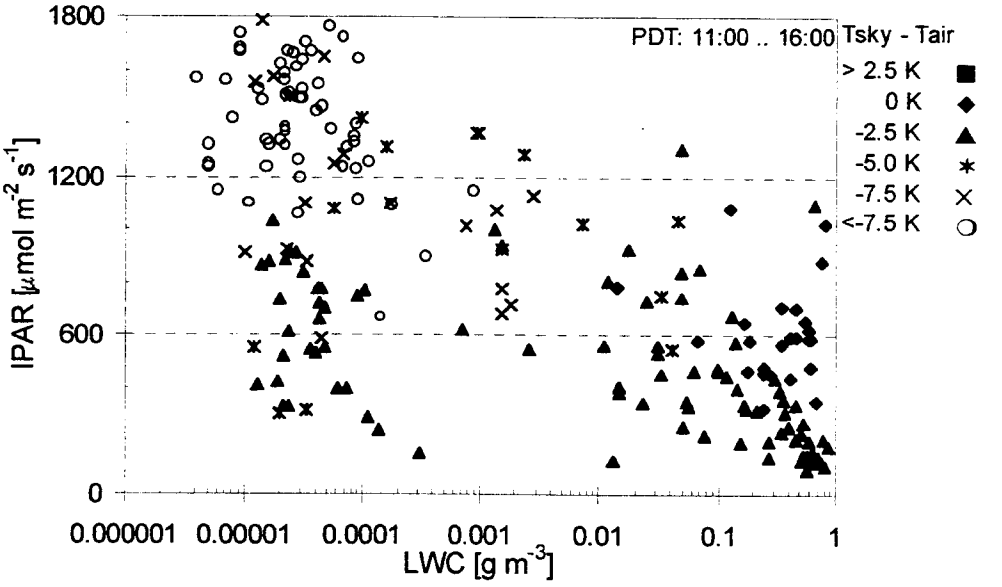

Figure 3.4 Midday (11:00 to 16:00 PDT) 28-minute mean PAR vs. cloud LWC

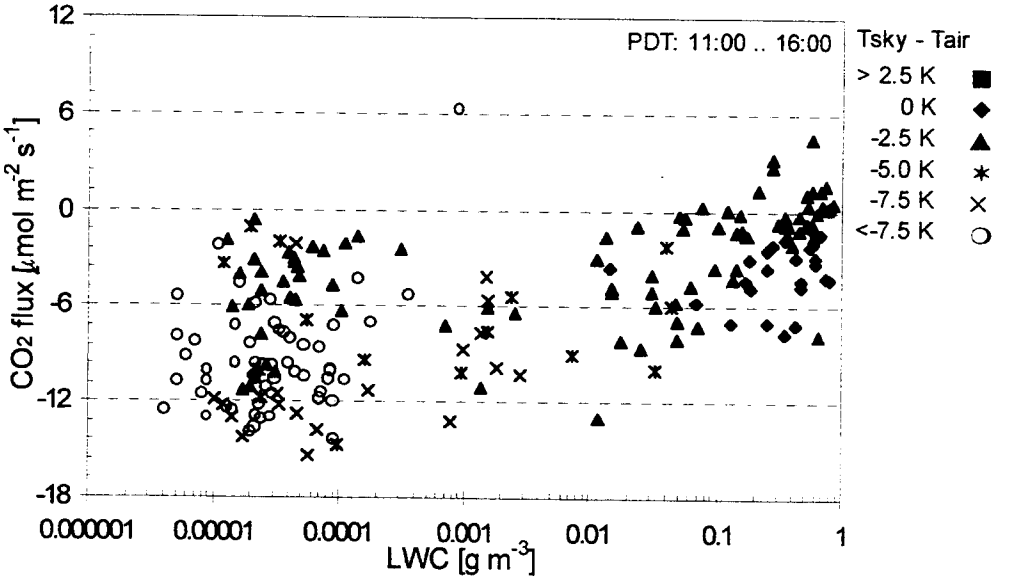

Figure 3.5 Midday (11:00 to 16:00 PDT) 28-minute CO_2 flux for non-cloudy and cloudy periods at Cheeka Peak

3.3.1 Days with High IPAR

For days with clear sky or high level clouds the midday incident PAR reached values well above 1200 µmol m^{-2} s^{-1}. Nine days in the period from Julian-day 223 to 262 satisfy a criterion of IPAR values well above 1200 µmol m^{-2} s^{-1} and wind direction in sector for most of the day: Julian days 225, 227, 230, 235, 241, 244, 247, 249, and 255. The Standard Screening procedure (see Section 2.11) was applied to the 28-minute-flux values of each day and the retained data averaged to hourly means. Data with unrealistic flux magnitudes of higher than 100 µmol m^{-2} s^{-1} were discarded. The values of all days for each hour were averaged and the standard deviation calculated. A sensitivity analysis to missing values for certain hours due to the Standard Screening procedure is presented in Appendix C and shows a small sensitivity for times, when large fluxes are encountered (midday or night). The hourly averaged CO_2 flux and

IPAR time traces for the days with high IPAR are shown in Figure 3.6 a) and b), respectively.

A high photosynthetically-driven downward net carbon flux is apparent from 10:00 to 18:00. The plant uptake of CO_2 increased steadily reaching maximum downward carbon flux values of -12 to -14 μmol m^{-2} s^{-1}, and a mean of around -11 μmol m^{-2} s^{-1} with a standard deviation of about 2 μmol m^{-2} s^{-1}. The integrated net carbon uptake over the whole day is about -0.2 mol m^{-2} day^{-1}, which is equivalent to -23.2 kg-C ha^{-1} day^{-1}. The mean respiration during the nighttime varies among 0.5 to 3 μmol m^{-2} s^{-1}.

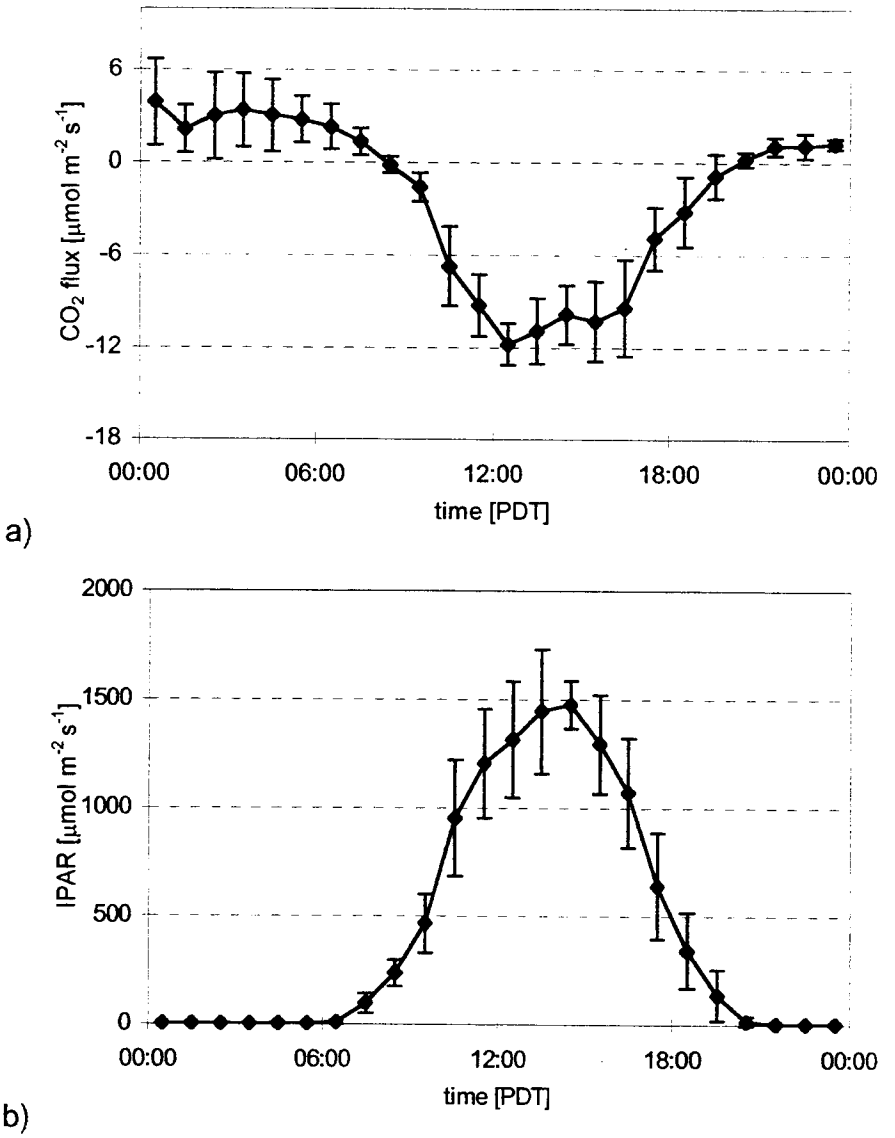

Figure 3.6 a) CO_2 flux and b) mean IPAR trend for days with high IPAR condition (hourly averaged values are plotted with error bars given by one standard deviation around the mean)

3.3.2 Days with Mid-range IPAR

The hourly averaged CO_2 flux and IPAR time traces for days with reduced incoming radiation are shown in Figure 3.7 a) and b). The reduction is most likely related to the presence of cloud overhead or surface cloud at the site,

which reduced the midday incoming PAR to mid-range photon fluxes between 600 to 1200 μmol m^{-2} s^{-1}. Eleven days show IPAR conditions in the mid-range regime; Julian-days 226, 228, 231, 232, 233, 236, 243, 245, 251, 253 and 261. The mean and standard deviation were calculated with the same scheme as in the high IPAR case (see section 3.3.1).

The mean net carbon uptake flux during peak IPAR hours reaches maximum values around -10 to -13 μmol m^{-2} s^{-1}, a mean of around -6 to -7 μmol m^{-2} s^{-1} (about two-third the flux magnitude as in the high IPAR case) and a standard deviation of ~3 μmol m^{-2} s^{-1}. The nighttime mean respiration agrees very well with the mean nighttime respiration of the high IPAR case, but shows less overall variance. The 24 hour integrated net exchange for the mid-range IPAR case results in a net carbon uptake of -0.09 mol m^{-2} day^{-1} or -10.5 kg-C ha^{-1} day^{-1}.

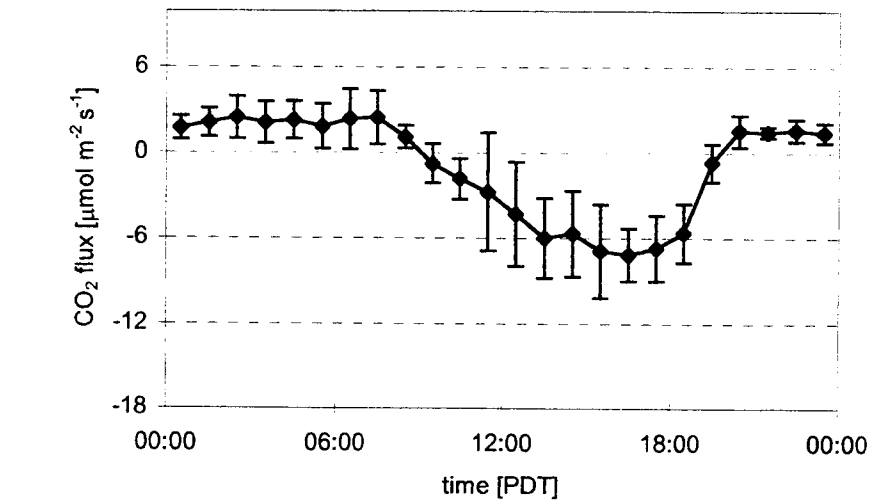

a)

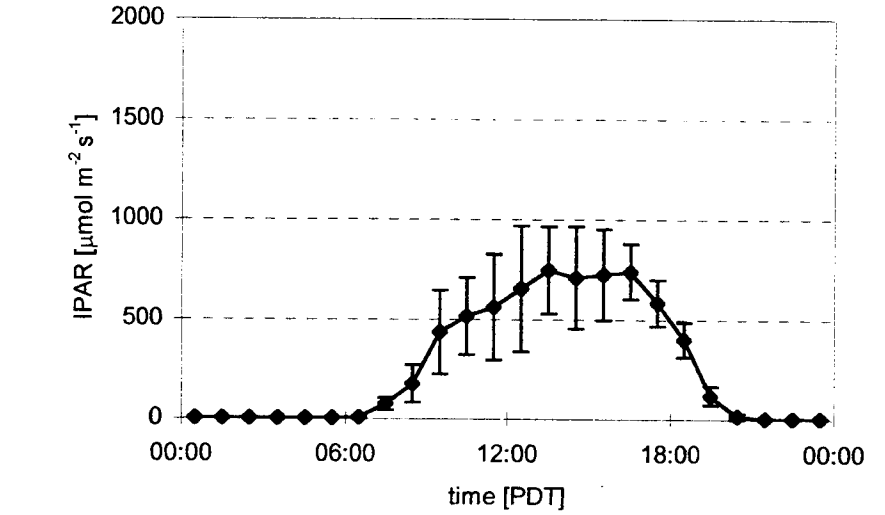

b)

Figure 3.7 a) CO_2 flux and b) mean IPAR for days with mid-range IPAR condition (hourly averaged values are plotted with error bars given by one standard deviation around the mean)

3.3.3 Days with Low IPAR

The few days with persistent low level or surface clouds throughout the whole day show a substantial reduction in incoming radiation compared to clear days. Six days had conditions of maximum IPAR values below 600 µmol m^{-2} s^{-1}

for the whole day: Julian-days 234, 246, 250, 252, 256, and 257. The mean and standard deviation were calculated with the same scheme as in the high IPAR case (see section 3.3.1). The hourly averaged carbon dioxide flux and IPAR time traces are shown in Figure 3.8 a) and b).

Photosynthesis is strongly dependent on incoming radiation and for the low IPAR case the photosynthetically-driven carbon uptake is very low, maximum downward flux values of -1.5 to -3 μmol m^{-2} s^{-1}. The hourly averaged net flux during peak IPAR hours stayed close to zero ($\approx$-0.5 μmol m^{-2} s^{-1}) (standard deviation in the data of around $\approx$1.5 μmol m^{-2} s^{-1}), which is indicating a near balance of photosynthesis and respiration. For a substantial decrease of PAR below the light compensation point the respiration term is larger than the photosynthesis and an upward flux (release of carbon) is encountered. In contrast to the mid-range and high IPAR case, the 24 hour integrated net exchange for the days with persistent low IPAR throughout the whole day resulted in a net carbon release of 0.05 mol m^{-2} day^{-1}, equivalent to 6.5 kg-C ha^{-1} day^{-1}.

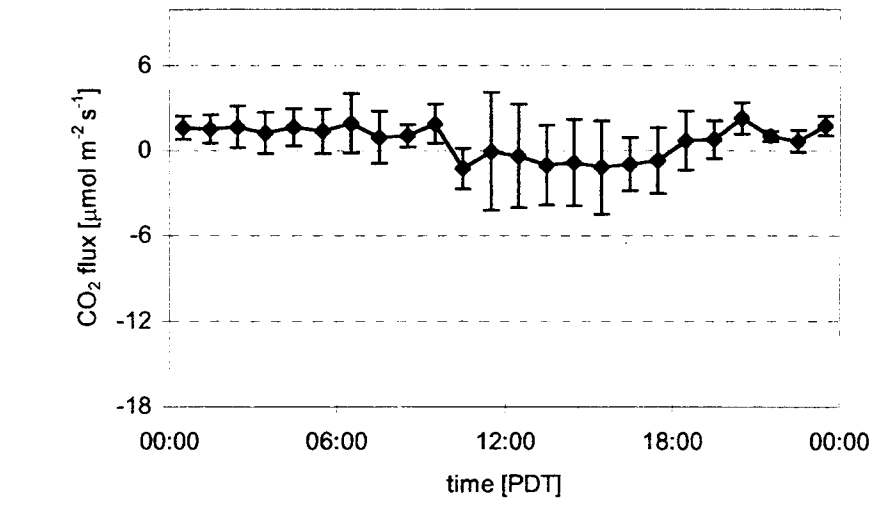

a)

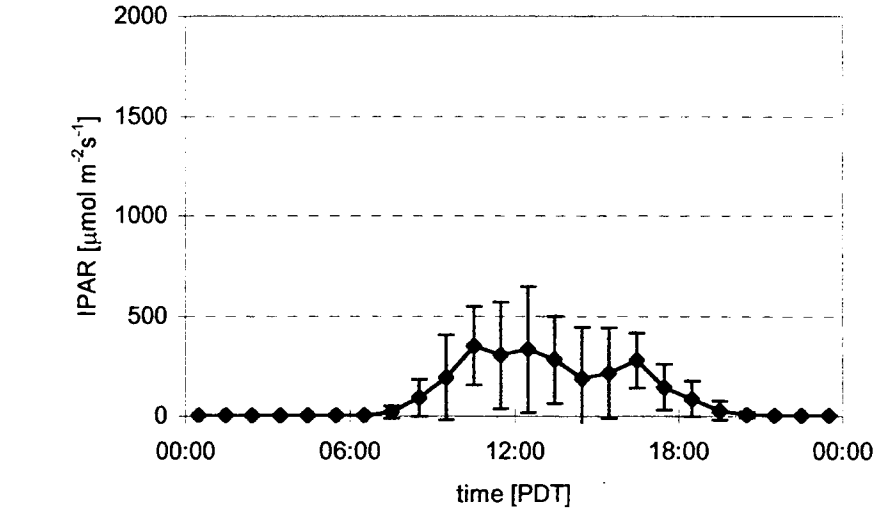

b)

Figure 3.8 a) CO_2 flux and b) mean IPAR for days with persistent low IPAR condition throughout the whole day (hourly averaged values are plotted with error bars given by one standard deviation around the mean)

3.4 Photosynthesis vs. IPAR

The photosynthesis of the canopy at Cheeka Peak showed a clear response to the incoming photosynthetically active radiation (IPAR). A total of 458 28-minute flux data points were available after applying the Standard Screening and screening for daytime (IPAR>5 μmol m^{-2} s^{-1}). The retained data include time periods with clear sky, high and low level cloud, or surface cloud at the site (LWC>0.01 g m^{-3}). As expected, the response curve has a strong increase for low IPAR values and gets into a saturation region for higher IPAR (see Figure 3.9, shown with plant physiological sign convention: upward respiratory flux negative and photosynthetically-driven downward flux positive).

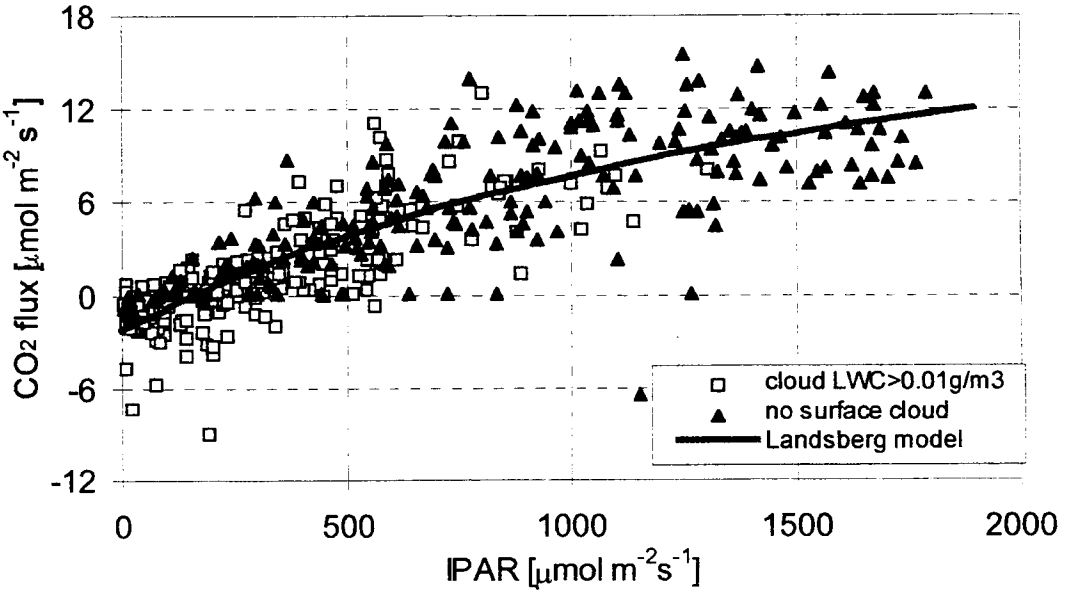

Figure 3.9 Light response curve of forest at Cheeka Peak

The Landsberg model parameters (eq. 3) were calculated with a least squares fitting method. A good correlation between CO_2 flux and IPAR was

found (r^2 = 0.7). The maximum photosynthetic rate (F_{max}) was 27.4 μmol m^{-2} s^{-1}, the dark respiration (R_d) was -2.3 μmol m^{-2} s^{-1}, and the quantum use efficiency (α_p) was 0.016 mol mol^{-1} (parameters are with plant physiological sign convention: upward respiratory flux negative and photosynthetically-driven downward flux positive).

3.5 Midday Photosynthesis vs. Vapor Pressure Deficit

In most plant species, large atmospheric water vapor pressure deficits (VPD) lead to a reduction in gas exchange through the leaf stomatal pores. This restricts the rate of transpiration and also reduces the rate of carbon dioxide uptake. Data collected in this study were analyzed whether this response occurred.

A total of 130 downward CO_2 flux observations are retained after applying the Standard Screening and limiting the time periods to higher IPAR values (> 600 μmol m^{-2} s^{-1}) and no cloud at the site (LWC < 0.01 g m^{-3}). The range of the vapor pressure deficit during those periods was generally less than 6 hPa. The vegetation at Cheeka Peak did not appear to respond to this small vapor pressure deficit. A slight increase in the downward CO_2 flux with increasing vapor pressure deficit can be seen in Figure 3.10a, but this is probably related to the positive correlation of increased VPD for higher IPAR levels (see Figure 3.10b), where carbon uptake is increased. The low vapor pressure deficit values can be attributed to the marine influence for winds in the sector 180° to 270°, which brings moist air from the ocean to the site.

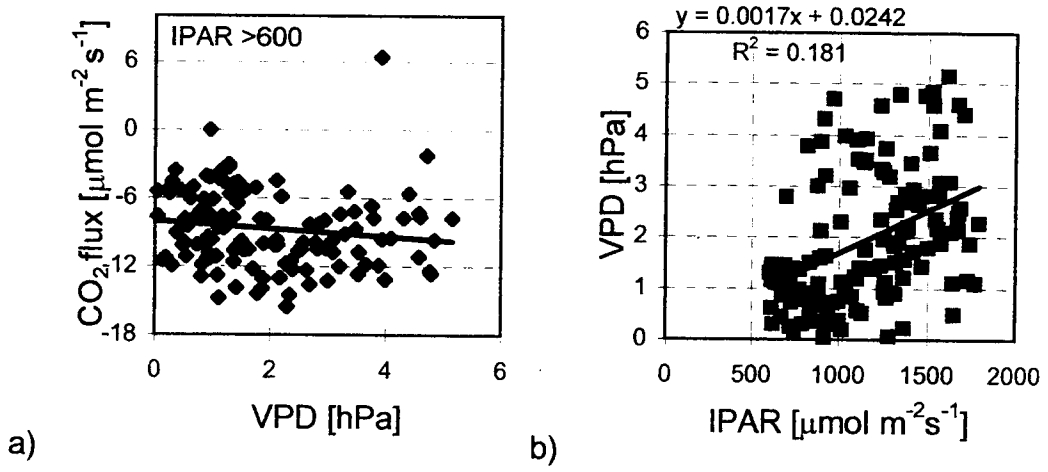

Figure 3.10 a) CO_2 Flux vs. VPD and b) VPD vs. IPAR for IPAR > 600 μmol m^{-2} s^{-1}

3.6 Respiration vs. Soil Temperature

Respiration occurs 24 hours per day. The analysis of the temperature dependence of respiration was limited to nighttime periods, when only respiration occurs and photosynthesis does not confound respiration estimates. The number of retained 28-minute flux time periods is 284, after applying the Standard Screening plus selecting for nighttime periods (IPAR < 5 μmol m^{-2} s^{-1}).

A definite relation between soil temperature and nighttime respiration is not apparent (r^2 < 0.08). This may be related to the small soil temperature range (10°C to 14.5°C) during the experimental period (see Figure 3.11). The average and standard deviation of all retained nighttime respiratory fluxes is 1.8 μmol m^{-2} s^{-1} and 1.5 μmol m^{-2} s^{-1}, respectively. The corresponding average soil temperature is 12.5 °C and the standard deviation in the soil temperature is 0.8 °C. The 24 hour integrated release of respired carbon for an assumed daily mean respiration of 1.8 μmol m^{-2} s^{-1} computes to 0.15 mol m^{-2} day^{-1} or 17.6 kg-C ha^{-1} day^{-1}.

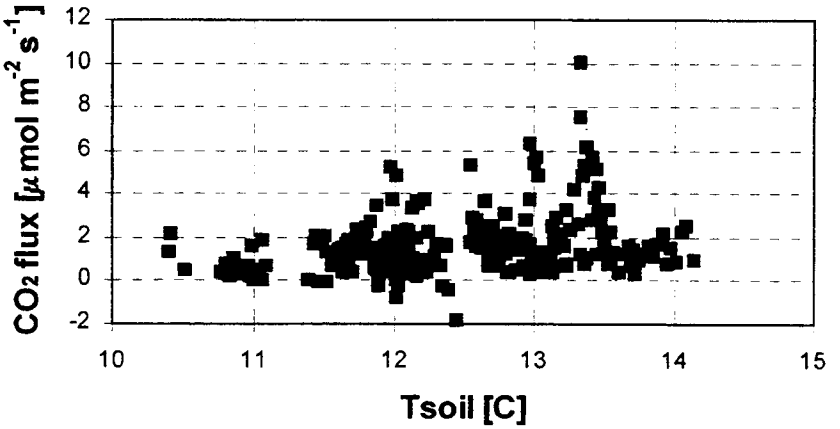

Figure 3.11 Nighttime respiration vs. soil temperature

Some negative (upward) flux values can be seen in the Figure 3.11, which are most likely caused by measurement errors attributed to the extreme wind conditions (wind speed > 11 m s^{-1}) during those time periods.

Some of the observed scatter in the data might be related to the dependence of the measured CO_2 flux on the upward mixing of the respired carbon dioxide from the canopy layer. Nights with no cloud at the site are generally in stable conditions (48 out of the 284 nighttime periods are without cloud at the site), and this will suppress vertical motion due to negative buoyancy and, hence, affect the exchange of respired CO_2 with the atmosphere. The observed eddy flux for those 48 time periods, at the instrument level, had a positive correlation to the friction velocity (u*) (see Figure 3.12b, $r^2 = 0.44$), a measure of the strength of turbulent mixing in the surface layer. Low u* (reduced turbulent mixing) leads to low values in the measured upward CO_2 flux, which is probably an underestimate of the ongoing respiration. For periods with low turbulent mixing (u* < 0.2 m s^{-1}) the measured CO_2 flux stayed below 1.5 μmol

m^{-2} s^{-1} and for well-mixed periods ($u^* > 0.2$ m s^{-1}, maximum observed value of 0.6 m s^{-1}) the measured respiration flux reached values of around 2.5 μmol m^{-2} s^{-1}.

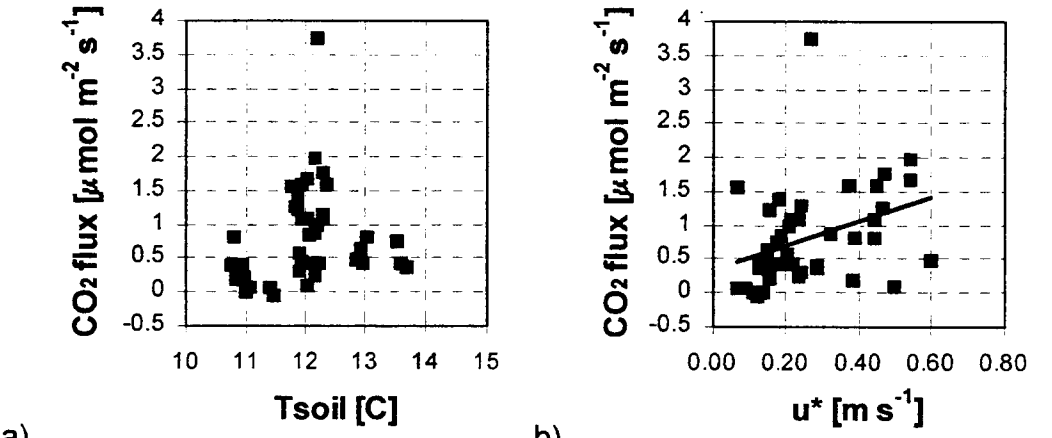

Figure 3.12 a) Nighttime respiration vs. soil temperature and b) vs. friction velocity (u^*) for time periods without surface cloud

For periods with surface cloud at the site, no definite correlation between the friction velocity and the measured respiratory CO_2 flux magnitude was observed (see Figure 3.13; $r^2<0.05$).

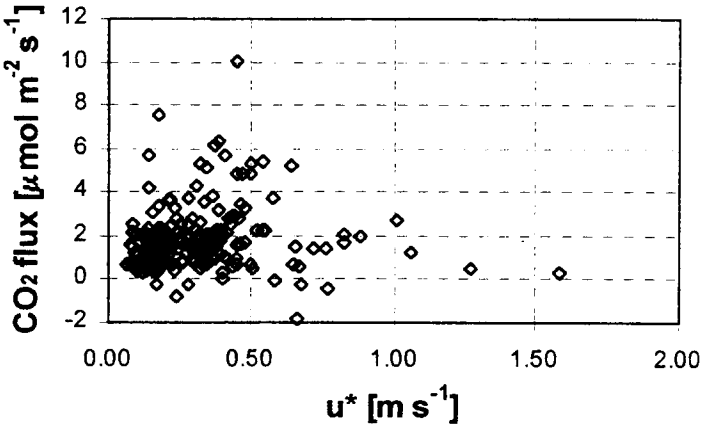

Figure 3.13 Nighttime respiration vs. friction velocity (u*) for time periods with surface cloud at the site

3.7 Energy Balance

A total of 270 daytime and nighttime net radiation, sensible and latent heat flux observations are retained after applying the Standard Screening and limiting the time periods to no cloud at the site (LWC < 0.01 g m^{-3}). The limitation to no surface cloud at the site is due to the generally unavailable information of the latent heat flux component for in cloud periods. The sensible heat flux and the soil heat flux plus heat storage are fairly well correlated (r^2 = 0.67 and r^2 = 0.74, respectively) to the net radiation (see Figure 3.14a and Figure 3.14a), where as the latent heat flux shows a small correlation (r^2 = 0.07) to the net radiation (see Figure 3.14b), probably related to measurement problems of the Kr hygrometer caused by the frequent interception of cloud droplets. A good energy balance closure in terms of net radiation equals the sum of sensible, latent and soil heat flux, and soil heat storage is not achieved (r^2=0.19, see Figure 3.15b), since no reliable information about the latent heat flux is available. The regression slopes show a partition of 46 percent and 5 percent of the incoming energy into the sensible heat and soil component of the energy

balance, respectively. The remaining 49 percent of the incoming energy should be mostly attributed to a latent heat flux component.

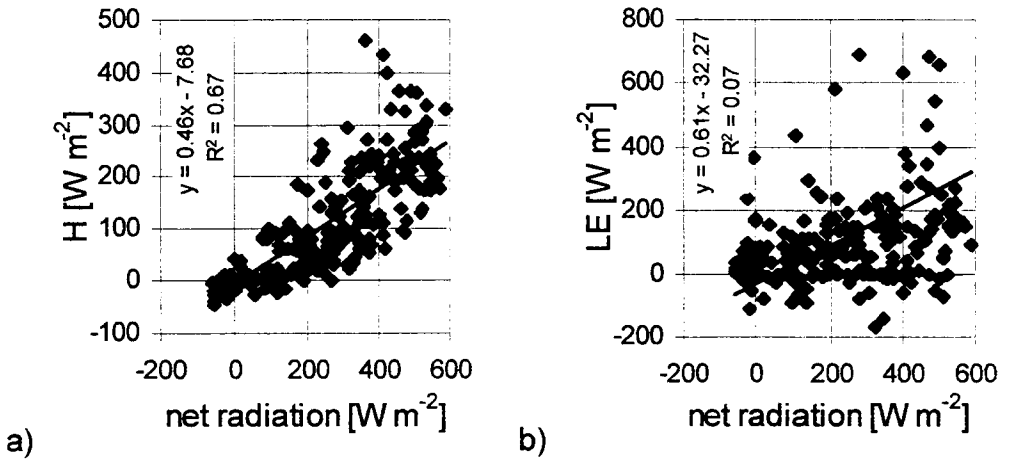

Figure 3.14 a) Sensible heat flux (H) and b) latent heat flux (LE) vs. net radiation (not shown are 3 latent heat flux data points with LE>960 W m^{-2} and 4 with LE<-440 W m^{-2})

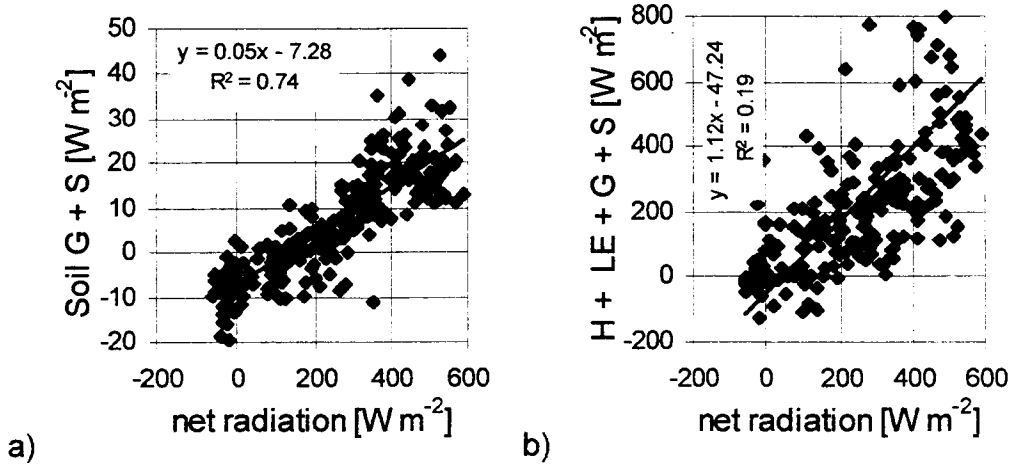

Figure 3.15 a) Soil heat flux (G) and heat storage (S) vs. net radiation and b) Sum of sensible (H), latent (LE), soil (G) heat flux and soil heat storage (S) vs. net radiation

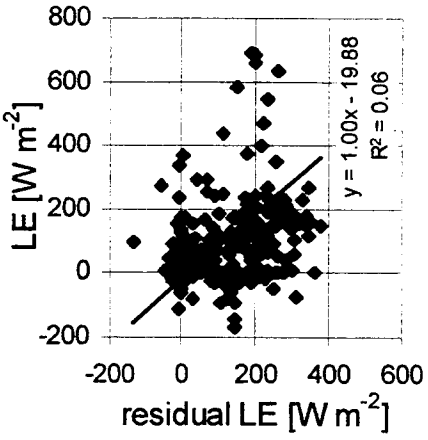

Figure 3.16 Measured latent heat (LE) vs. residual latent heat flux

4. Discussion

4.1 Environmental Factors Controlling the Carbon Dioxide Exchange

The carbon dioxide exchange at Cheeka Peak during August and September 1994 showed a clear diurnal pattern for days with significant amount of incoming radiation. The maximum midday net CO_2 fluxes and the 24 hour integrated carbon exchange between the forest and the atmosphere are shown in Table 4.1 for three distinctive incoming PAR regimes. The daily net fixation for days with a significant amount of incoming radiation (clear sky, partial cloud or thin cloud conditions) is less than the carbon accumulation of ~0.5 mol m^{-2} day^{-1} found at Harvard Forest, Massachusetts, for the time period around August 1994 (Goulden et al., 1996c), but comparable to the carbon accumulation of ~0.09 mol m^{-2} day^{-1} for the dry season in 1992 at an undisturbed tropical rain forest (Grace et al., 1995a) and comparable to the net exchange of ~0.13 mol m^{-2} day^{-1} of a boreal forest during Summer 1994 (Goulden et al., 1996b).

Table 4.1 Daytime net CO_2 exchange for three IPAR regions

midday IPAR range	**possible cloud condition**	**midday mean and peak CO_2 flux**	**24 hour integrated net exchange**
μmol m^{-2} s^{-1}		mean μmol m^{-2} s^{-1}, (peak) μmol m^{-2} s^{-1}	mol m^{-2} day^{-1}, (kg-C ha^{-1} day^{-1})
> 1200	Clear sky or high level cloud	-11, (-12 to -14)	-0.19, (-23.3)
600 to 1200	Partial cloud cover or thin cloud	-6.5, (-10 to -13)	-0.09, (-10.5)
< 600	Thick low level or surface cloud	≈ -0.5, (-1.5 to -3)	0.05, (+6.5)

A comparison of the Cheeka Peak photosynthetic light response parameter with those of other forests is shown in (see Table 4.2). The quantum use efficiency of Cheeka Peak is comparable to the α_p of the coniferous Black Spruce forest, but lower than the α_p of the deciduous forests. This may be related to the necessity of deciduous forest to gain carbon during a shorter leaf-on period than coniferous species, which carry leaves year round. The same reasoning may explain the lower maximum attainable photosynthetic rate (F_{max}) at Cheeka Peak compared to the deciduous species.

Table 4.2 Comparison of Cheeka Peak photosynthetic light response data with other forests, where α_p = quantum use efficiency, F_{max} = maximum attainable photosynthetic rate, R_d = dark respiration in the low light limit; [1] light response curve from Gross CO_2 exchange

Reference	Forest	α_p	F_{max}	R_d	r^2
		$\frac{mol}{mol}$	$\frac{\mu mol}{m^2 s}$	$\frac{\mu mol}{m^2 s}$	
This study, Summer 1994	coniferous (Silver fir and Western hemlock), 24 years old	0.016	27.4	-2.3	0.71
Wofsy et al., 1993 Summer 1991	mixed deciduous, 50- to 70- years old	0.039	28.0	-4.0	NA
Goulden et al., 1996a [1] Summer 1992	(same as in Wofsy et al., 1993, see above)	0.055	32.9	-1.4	NA
Hollinger et al., 1994 Summer 1990	deciduous (Red beech), > 300 years old	0.043	14.2	-4.5	0.44
Hollinger et al., 1994 Late Summer 1990	deciduous (Red beech), > 300 years old	0.023	31.1	-4.1	0.58
Fan et al., 1995 Summer 1990	coniferous (Black spruce), 200 years old	0.017	NA	NA	NA

An influence of the atmospheric saturation vapor pressure deficit on the plants daytime net carbon uptake was not observed; this is probably related to the generally low-VPD (below 6.5 hPa) due to the marine influence on the site. The VPD below 6 hPA compares very well to the VPD (3 to 6hPa) found at Fetteresso, a site in an oceanic climate (Jarvis et al., 1976). Hollinger (1993) and Fan et al. (1995) show a reduction in the carbon dioxide uptake for higher VPD (10 hPa to 20 hPa), and Law and Waring (1994) show a stomatal closure for VPD greater than ~25 hPa for Douglas Fir and shrubs.

A clear dependence of the nighttime respiration on temperature was not apparent; this is probably related to the narrow soil temperature range of 10 to 14.5 °C throughout the experiment. Goulden et al. (1996a) detected that nocturnal net ecosystem exchange over a whole year was exponentially related to surface soil temperature with a total range from -1 to 21 °C , the range of the Cheeka Peak nocturnal NEE coincides very well with the data of the Harvard forest in the temperature sub-range from 10 to 15 °C. For stable conditions a positive correlation of measured nighttime CO_2 fluxes to the strength of turbulent mixing (characterized by the friction velocity, u*) suggest a possible suppression of the measured CO_2 eddy flux due to stability, which is in agreement with the results found at Harvard forest (Goulden et al., 1996a). A flushing out of accumulated CO_2 during stable night conditions, due to the onset of turbulence in the morning hours, was not detected at the eddy flux station. This suggests either a good coupling of the forest to the atmosphere or removal of the respired CO_2 by advection or cold air drainage down the slope. For periods with surface cloud at the site, generally in neutral conditions, higher CO_2 flux magnitudes were encountered than for periods without surface cloud, suggesting a good coupling of the forest to the atmosphere under those cloud conditions. The Landsberg model dark respiration (R_d) parameter (2.3 μmol m^{-2} s^{-1}) agrees very well with the observed mean nighttime respiration rate of 1.8±1.5 μmol m^{-2} s^{-1}.

4.2 Comparison with Available Leaf Photosynthesis Research Data

In fall 1993 a lab-based light response curve study was undertaken by Martin (1993, unpublished data) on "current" leaves (sun grown in spring 1993) of two *A. amabilis* stands close to Seattle, WA. One stand is about 38 years old (1140 m elevation, 7 m average tree height), the other is about 45 years old (1300 m elevation, 14 m average tree height, LAI of 9, BA of 94.8 m^2 ha^{-1}). The light response curve saturated for high PAR at 3.6 μmol m^{-2} s^{-1} for the 38 year-old stand and 4.6 μmol m^{-2} s^{-1} for the 45 year-old stand (values are on a one-sided leaf area basis and illumination of the leaves was from the top only). A simple scaling to obtain an estimate of a theoretical achievable maximum canopy photosynthesis is possible according to (Landsberg, 1986)

$$P_{canopy} = P_{leaf} * LAI \qquad (46)$$

where P_{canopy} is the theoretically achievable net CO_2 uptake of the canopy on a per ground area basis without consideration of soil, root and stem respiration, P_{leaf} is the net CO_2 uptake of the foliage on one-sided leaf area basis, LAI is the leaf area index (total projected leaf area per unit area of ground).

With the assumption of a leaf area index of around 7 (leaf area index at Cheeka Peak), a theoretical maximum net CO_2 uptake per ground area of about 28 μmol m^{-2} s^{-1} would be expected. In reality, *A. amabilis* trees gain carbon from a variety of leaf age classes and leaf photosynthesis declines with foliage age, seven years old foliage has about half the capacity of one year old (Teskey et al., 1983), and in addition not all leaves of a forest are illuminated equally. Hence, the expected carbon uptake should clearly be below the theoretical maximum rate of 28 μmol m^{-2} s^{-1}. Assuming an even spaced distribution of leaf age and a linear decline in leaf photosynthesis from a one-year-old leaf rate of 28 μmol m^{-2} s^{-1} to a seven-year-old leaf rate of 14 μmol m^{-2} s^{-1}, results in an expected canopy photosynthetic rate of about 21 μmol m^{-2} s^{-1}. In addition,

assuming an exponential decline of leaf illumination with distance into the canopy results in a further reduction of the expected photosynthetic rate to about 60 to 70 percent of the age-weighted rate. This scaling estimate suggests, the measured mean carbon uptake of the canopy at Cheeka Peak in the high IPAR case (~11 μmol m^{-2} s^{-1}) is about 70 percent of a theoretical expected uptake of an *A. amabilis* canopy with LAI comparable to the LAI at Cheek Peak.

The initial slope of the measured leaf light response curve data, the apparent quantum-use efficiency α_p for the 45-year old was 0.025 mol mol^{-1} (estimated from four leaf photosynthesis vs. IPAR data points) and 0.055 mol mol^{-1} for the 38-year old stand (only two data points were available in low IPAR region). The α_p estimate of the 45-year old stand is comparable (slightly higher) to the 0.016 mol mol^{-1} found at Cheeka Peak, whereas the 38-year old stand has a much higher value, but the quantum use efficiency was estimated from two data points only.

4.3 Validity of Steady State and Horizontal Homogeneity Assumptions

The mean carbon dioxide exchange source/sink strength (S_c) of the forest at Cheeka Peak was calculated with the assumptions of steady state (small change of CO_2 concentration with time) and horizontal homogeneous, according to

$$S_c = \overline{w'C'}_{10m} \qquad (47)$$

where $\overline{w'C'}_{10m}$ is the measured net CO_2 flux at the 10m level, and S_c is the source or sink strength of the forest ($S_c < 0$ forest is a sink for CO_2, $S_c > 0$ forest releases carbon dioxide).

Under conditions, with a significant amount of incoming radiation, the forest would fix carbon dioxide out of the atmosphere at a rate of -10 μmol m^{-2}

s^{-1}. For early morning or evening periods the plant uptake would be around -1.0 $\mu mol\ m^{-2}\ s^{-1}$ and for nighttime periods the plant system would respire CO_2 on the average at a rate of 1.8 $\mu mol\ m^{-2}\ s^{-1}$.

A deviation from steady state, change of the carbon dioxide concentration with time, might contribute to the CO_2 exchange of the plant system. During stable nighttime conditions the CO_2 concentration in the canopy layer could increase due to respiration, and in the early morning hours a decrease of the stored CO_2 in the canopy layer due to photosynthesis would take place. This "recycled" CO_2 is not measured by the eddy correlation system above the canopy layer, but during the early morning onset of turbulence some of the stored CO_2 should be flushed out of the layer and detected as a CO_2 flux spike at the eddy flux measurement level.

The importance of the time rate change in the stored CO_2 to the carbon exchange for early morning hours can be estimated with a worst case scenario of a -10 $\mu l\ l^{-1}$ change in CO_2 over a 2 hour period, according to

$$S_{storage} = \frac{\partial \overline{C}}{\partial t} h \qquad (48)$$

where $\frac{\partial \overline{C}}{\partial t}$ is the mean storage of carbon dioxide, and h is a typical vertical length due to an integration of the storage term, which is assumed to be constant with height. The change of -10 $\mu l\ l^{-1}$ is a generally high value for the difference in the midnight to noon mean CO_2 concentration measured above the forest and the 2 hour period reflects the early morning transition time from a positive respiration flux to a photosynthesis related negative CO_2 flux. These assumptions would lead to a change in the CO_2 storage , after integration over the canopy layer, in the order of -0.6 $\mu mol\ m^{-2}\ s^{-1}$. If the time for the 10 $\mu l\ l^{-1}$ change would be taken about 12 hours (midnight to noon) the change in the CO_2 storage would be of the order of -0.1 $\mu mol\ m^{-2}\ s^{-1}$. This uptake is not associated with a downward flux of CO_2 into the forest and would be undetected at the eddy

flux measurement level. For the evening transition from day to night the change should be of comparable magnitude, but opposite in sign.

For morning or evening time periods the change in CO_2 storage could be of the order of 10 to 60 percent of a typically eddy flux input of -1 $\mu mol\ m^{-2}\ s^{-1}$, leaving the eddy flux as the main contributor of CO_2 for the forest. For midday or midnight time the change in the CO_2 concentration over time is much smaller and therefore the change in storage as well.

At a site in the Amazon region, Grace et al. (1995b) found that the change in the CO_2 concentration was important to compensate for the characteristic early morning CO_2 flush out, detected as an upward spike in the measured CO_2 eddy flux. The CO_2 eddy flux at Cheeka Peak does not show this characteristic feature, suggesting either a good coupling of the canopy layer to the atmosphere or a removal of the respired CO_2 by another process, such as cold air drainage down the slope or advection inland by the mean wind.

A change in the horizontal surface structure, such as transition from ocean to vegetated land, might be important for net CO_2 exchange. Advection of carbon dioxide by the mean wind could occur. An estimate of the possible magnitude of the advection effect (S_{adv}) is given by

$$S_{adv} = \bar{u}\frac{\partial \overline{C}}{\partial x}h \qquad (49)$$

where $\bar{u}$ is the mean wind speed, $\frac{\partial \overline{C}}{\partial x}$ is the horizontal CO_2 concentration gradient, and h is a typical vertical length due to an integration of the advection term, which is assumed to be constant with height.

Under the assumption of "no exchange of CO_2 between the ocean and the atmosphere above it", the CO_2 concentration in the air coming from the ocean would lie around the estimated 24-hour ambient mean value of 353 $\mu l\ l^{-1}$. A 5 $\mu l\ l^{-1}$ lower midday concentration (1/2 the 10 $\mu l\ l^{-1}$ day-night difference) 4 km inland at Cheeka Peak measured at the 10 m level and a typical mean wind of

5 m s^{-1} would result in an input of the order of S_{adv} = -2.8 μmol m^{-2} s^{-1} into the plant system. For nighttime the gradient would be in the opposite direction resulting in an input of S_{adv} = +2.8 μmol m^{-2} s^{-1}. This input is about 30 percent of the measured midday eddy flux input of -10 μmol m^{-2} s^{-1} and comparable to nighttime eddy flux values around 1.8 μmol m^{-2} s^{-1}.

Advection effects are only relevant a limited distance from the surface change. As a rule of thumb, 100 m fetch for each 1 m above the effective surface is required to adjust the atmospheric layer to the new surface features (Baldocchi et al., 1988). In the case of Cheeka Peak, with a distance of 4 km to the ocean, the layer depth adapted to the underlying vegetated surface would be about 40 m. The measurement level at 4 m above the trees would clearly be inside this adjusted boundary layer and advection of CO_2 from the ocean should have negligible effect on the net exchange.

5. Summary and Conclusions

During summer 1994 the 3rd field intensive of the NSF-funded Cloud and Aerosol CHemistry Experiment (CACHE) was performed at Cheeka Peak in Washington. The Cheeka Peak research site is located on top of a 463 m high North-South extending ridge, the terrain falls off steeply to the East, South and West with an average slope of about 17°. The terrain on the West-Southwest sector of the mountain is fairly homogeneous, descending with some smaller rolling hill sections.

Net surface fluxes at Cheeka Peak were measured with the eddy correlation technique. The net surface fluxes of carbon dioxide, sensible heat, and latent heat were calculated from the time-averaged covariance of measured wind speed and fluctuations of CO_2 concentration, temperature, and water vapor. Wind speed data, measured with a sonic anemometer, were preprocessed with a despiking routine, detrended by a running-mean high-pass filter with a time constant of 200 seconds, and rotated to align the calculated flux normal to the streamline. The measured scalars, carbon dioxide, water vapor, and temperature, were detrended with the same running-mean high-pass filter procedure. Fluxes were calculated on a ~28 minute basis. The selection of valid flux periods for further analysis was based on a "Standard Screening" criteria that involved: limitation of the wind direction to the sector 180 ° to 270 ° to ensure minimal influence of non-homogeneous regions, rejection of time periods with a large number of detected spikes (f > 1 %) in the sonic wind speed data, and exclusion of system maintenance time periods. 742 twenty-eight-minute flux periods out of a total of 1959 were retained after applying the Standard Screening criteria. The retained time periods consist of 62 percent daylight (IPAR>5 μmol m^{-2} s^{-1}) and 38 percent nighttime data. Surface cloud at the site (LWC>0.01 g m^{-3}) occurred on 49 percent of the daylight time periods and 83 percent of the nighttime periods. The analysis of the derived fluxes were

supported with standard meteorological and physiological measurements, including short wave, long wave, and photosynthetically active radiation, air temperature and relative humidity, wind speed and direction, soil temperature and soil heat flux.

Energy balance closure was not achieved due to the lack of reliable latent heat fluxes, related to measurement problems of the krypton hygrometers due to the frequent interception of cloud water. A clear linear relation of the sensible heat and soil energy balance component and the net radiation was found. The net radiation energy was partitioned into 46 percent sensible heat flux and 5 percent soil heat flux and storage. The residual of 49 percent should mostly be attributed to the latent heat component in the energy balance.

The response of the net ecosystem CO_2 exchange to environmental factors governed by the marine influence and the complex topography was investigated. The expected variation of nighttime respiratory flux with temperature was undetectable, because of the small soil temperature range of 10 to 14.5 °C encountered throughout the experiment period. The mean nighttime respiration for the entire experiment was 1.8 $\mu mol\ m^{-2}\ s^{-1}$ with a standard deviation of 1.5 $\mu mol\ m^{-2}\ s^{-1}$. Suppression of mixing on nights with expected stable atmosphere condition was indicated by the positive correlation of the measured nighttime eddy CO_2 flux to the friction velocity (u^*), a measure of the turbulent mixing.

A constraining influence of the atmospheric saturation vapor pressure deficit on the plants daytime net carbon uptake was not observed, which is clearly related to the marine influence for winds coming from the ocean. The advection of moist marine air to the site leads to a vapor pressure deficit generally below 6.5 hPa, values too small to cause a significant leaf stomatal closure and an associated photosynthesis shutdown. This shutdown would probably occur for wind conditions bringing dry continental air to the site.

A clear diurnal pattern, uptake of carbon during the day and release of carbon at night, was found for days with substantial input of photosynthetically

active radiation (high and mid-range IPAR cases). Attenuation in the incoming PAR due to cloud cover resulted in an observed reduction in the carbon uptake of the plants. For a large decrease in IPAR, due to persistent low level or surface cloud during daylight hours, net photosynthesis was strongly reduced and only a small downward or even an upward CO_2 flux was detected.

The strong response of the measured CO_2 eddy flux to incoming photosynthetically active radiation clearly shows the appropriateness of using the eddy correlation technique to evaluate the CO_2 net exchange of the plant system.

A comparison with leaf photosynthesis research data (scaled-to-per-ground-area) of the dominant tree species (*Abies amabilis*), suggested the measured eddy carbon fluxes might underestimate the net ecosystem exchange by 30 percent, assuming the same physiological light response. Since an adaptation of a forest to existing meteorological and physiological factors can be expected, a different light-response of the trees at Cheeka Peak is possible. The disagreement of predicted to measured carbon uptake leads to the need of an accuracy check of the measured flux magnitude.

Supportive "spot" measurements (not necessarily continuous over the experiment duration) should be performed to evaluate the accuracy of the results from the eddy correlation technique. A respiration flux estimate could be obtained by performing chamber based measurements on the various sources (soil, roots, stems and leaves) contributing to the respired CO_2, but care has to be taken not to alter the microenvironment of the objects under study. Lab based leaf photosynthesis measurements, taken under controlled conditions (IPAR, Temperature, vapor pressure deficit), can shine light on the photosynthetic capacity of the entire canopy.

Measurements of the mean horizontal carbon dioxide gradient could be used to determine the importance of the simplifying assumption of horizontal homogeneity. To evaluate the contribution of the change in stored carbon dioxide in the plant layer to the carbon dioxide net exchange, a carbon dioxide

concentration profile would be necessary. The vertically integrated time change of the mean CO_2 concentration in the canopy layer would give an estimate of the amount of respired or taken-up carbon dioxide not seen by an above-canopy eddy flux system. At night in sloping terrain cold air drainage can lead to a removal of respired CO_2 down the slope. This removed carbon dioxide would not be detected by the slow response concentration profile system nor by the above-canopy eddy flux system. To evaluate the occurrence and importance of this process, it would be necessary to have information of the in-canopy-layer wind direction and wind speed.

A determination of the precision of the eddy flux calculated from the sonic and closed-path analyzer system would be possible by comparison with a sonic and open-path analyzer system. This comparative precision check would best be performed *in situ* for the ecosystem system under study, and for a duration of a few days, to reflect the possible multitude of environmental conditions.

Overall the net exchange of carbon dioxide between a forest system located in complex terrain and the atmosphere, as measured with the eddy correlation technique, showed a clear response of the forest to the amount of incident photosynthetically active radiation. The proximity to the ocean, and prevailing moisture-laden winds from the ocean, had a strong influence on the photosynthetic rate of the plant system. Frequently occurring, low level clouds lead to a reduction of incident photosynthetically active radiation at the surface and consequently a lower photosynthetic CO_2 uptake by the plants. Vapor pressure deficit did not appear to constrain the stomatal conductance and the photosynthetic process. To have a better understanding of the net ecosystem exchange, supportive measurements should be under taken to address the accuracy and precision of the eddy correlation flux system and check the validity of simplifying assumptions (steady state and horizontal homogeneity).

Bibliography

Applied Technologies (1992). Operator's manual: For SWS-211/3K three axis sonic wind system anemometer/thermometer. 6395 Gunpark Dr. Unit E, Boulder, CO 80301, Applied Technologies, Inc.

Baldocchi, D. D., B. B. Hicks and T. P. Meyers (1988). "Measuring Biosphere-Atmosphere Exchanges of Biologically Related Gases with Micrometeorological Methods." Ecology 69 (5): 1331-1340.

Baldocchi, D. D. and T. P. Meyers (1991). "Trace Gas Exchange Above the Floor of a deciduous Forest: 1. Evaporation and CO2 Efflux." Journal of Geophysical Research 96: 7271-7285.

Businger, J. A., W. F. Dabberdt, A. C. Delany, T. W. Horst, C. L. Martin, S. P. Oncley and S. R. Semmer (1990). "The NCAR Atmosphere-Surface Turbulent Exchange Research (ASTER) Facility." American Meteorological Society 71 (7): 1006-1011.

Campbell, G. S. and B. D. Tanner (1985). A Krypton Hygrometer for Measurement of Atmospheric Water Vapor Concentration. International Symposium on Moisture and Humidity, Instrum. Soc. Am., Research Triangle Park, N. C.

Chason, J. W., D. D. Baldocchi and M. A. Huston (1991). "A comparison of direct and indirect methods for estimating forest canopy leaf area." Agricultural and Forest Meteorology 57: 107-128.

Conway, T. J., P. Tans, L. S. Waterman, K. W. Thoning, D. R. Kitzis, K. A. Masarie and N. Zhang (1994). "Evidence for interannual variability of the carbon cycle from the National Oceanic and Atmospheric Administration/Climate Monitoring and Diagnostics Laboratory global air sampling network." Journal of Geophysical Research 99: 22831-22856.

Fan, S.-M., M. L. Goulden, J. W. Munger, B. C. Daube, P. S. Bakwin, S. C. Wofsy, J. S. Amthor, D. R. Fitzjarrald, K. E. Moore and T. R. Moore (1995). "Environmental controls on the photosynthesis and respiration of a boreal lichen woodland: a growing season of whole-ecosystem exchange measurements by eddy correlation." Oecologia 102 (4): 443-452.

Gill Instruments (1992). Solent Research Ultrasonic Anemometer, Product Specification. Lymington, Cannon Street, Hampshire, S041 9BR, Gill Instruments Ltd. (Solent House).

Goulden, M. L., J. W. Munger, S.-M. Fan, B. C. Daube and S. C. Wofsy (1996a). "Measurements of carbon sequestration by long-term eddy covariance: methods and critical evaluation of accuracy." Global Change Biology 2: 101-114.

Goulden, M. L., B. C. Daube, S.-M. Fan, D. J. Sutton, A. Bazzaz, J. W. Munger and S. C. Wofsy (1996b). Environmental Controls on the Carbon balance of a Boreal Forest: Annual Cycle of CO_2 Exchange measured be Eddy Covariance. Conference on Agricultural and Forest Meteorology.

Goulden, M. L., J. W. Munger, S.-M. Fan, B. C. Daube and S. C. Wofsy (1996c). "Exchange of Carbon Dioxide by a Deciduous Forest: Response to Interannual Climate Variability." Science: accepted 17 January 1996.

Grace, J., J. Lloyd, J. McIntyre, A. C. Miranda, P. Meir, H. S. Miranda, C. Nobre, J. Moncrieff, J. Massheder, Y. Malhi, I. Wright and J. Gash (1995a). "Carbon Dioxide Uptake by an Undisturbed Tropical Rain Forest in Southwest Amazonia, 1992 to 1993." Science 270: 778-780.

Grace, J., J. Lloyd, J. McIntyre, A. C. Miranda, P. Meir, H. S. Miranda, J. Moncrieff, J. Massheder, I. Wright and J. Gash (1995b). "Fluxes of carbon dioxide and water vapour over an undisturbed tropical forest in south-west Amazonia." Global Change Biology 1: 1-12.

Hojstrup, J. (1993). "A statistical data screening procedure." Measurement Science and Technology 4: 153-157.

Hollinger, D. Y., F. M. Kelliher, J. N. Byers, J. E. Hunt, T. M. McSeveny and P. L. Weir (1994). "Carbon dioxide exchange between an undisturbed old-growth temperate forest and the atmosphere." Ecology 75 (1): 134-150.

Jarvis, P. G., G. B. James and J. J. Landsberg (1976). Coniferous Forest. Vegetation and the Atmosphere. J. L. Monteith. New York, Academic Press. 2: 171-240.

Jarvis, P. G. and J. W. Leverenz (1983). Productivity of Temperate, Deciduous and Evergreen Forest. Physiological Plant Ecology IV: Ecosystem Processes: Mineral Cycling, productivity and Man's Influence. A. Pirson and M. H. Zimmerman. Berlin Heidelberg New York, Springer-Verlag. 12D: 233-280.

Jones, H. G. (1992). Plants and microclimate: a quantitative approach to environmental plant physiology, Cambridge University Press, Great Britain.

Landsberg, J. J. (1986). Physiological Ecology of Forest Production, Academic Press INC.

Law, B. E. and R. H. Waring (1994). "Combining remote sensing and climatic data to estimate net primary production across oregon." Ecological Applications 4(4): 717-728.

Leuning, R. and K. M. King (1992). "Comparison of Eddy-Covariance Measurements of CO_2 Fluxes by Open- and Closed-Path CO_2 Analysers." Boundary-Layer Meteorology 59: 297-311.

Leuning, R. and J. Moncrieff (1990). "Eddy-covariance CO_2 flux measurements using open- and closed-path CO_2 analysers: corrections for analyser water vapour sensitivity and damping of fluctuations in air sampling tubes." Boundary-Layer Meteorology 53: 63-76.

Martin, T. and T. M. Hinckley (1995). Personal Communication (04/21/95): Abies amabilis physiological information: sun-formed foliage light response curve data.

McMillen, R. T. (1988). "An Eddy Correlation Technique with Extended Applicability to Non-simple Terrain." Boundary-Layer Meteorology 43: 231-245.

Monteith, J. L. and M. H. Unsworth (1990). Principles of environmental physics. London.

Ryan, M. G. (1991). "A simple method for estimating gross carbon budgets for vegetation in forest ecosystems." Tree Physiology 9: 255-266.

Stull, R. B. (1988). An introduction to boundary layer meteorology, Kluwer Academic Publishers.

Teskey, R. O., C. C. Grier and T. M. Hinkley (1984). "Change in photosynthesis and water relations with age and season in Abies Amabilis." Can. J. For. Res. 14: 77-84.

Teskey, R. O., D. W. Sheriff, D. Y. Hollinger and R. B. Thomas (1995). External and Internal Factors Regulating Photosynthesis. Resource Physiology of Conifers: Acquisition, Allocation, and Utilization. W. K. Smith and T. M. Hinckley, Academic Press: 105-140.

Waring, R. H. and J. F. Franklin (1979). "Evergreen forests of the Pacific Northwest." Science 204: 1380-1386.

Webb, E. K., G. I. Pearman and R. Leuning (1980). "Correction of flux measurements for density effects due to heat and water vapour transfer." Quart. J. R. Met. Soc 106: 85-100.

Wofsy, S. C., M. L. Goulden, J. W. Munger, S.-M. Fan, P. S. Bakwin, B. C. Daube, S. L. Bassow and F. A. Bazzaz (1993). "Net Exchange of CO_2 in a Mid-Latitude Forest." Science 260: 1314-1317.

Appendices

Appendix A Influence of the Detrending Filter Time Constant on the CO_2 Eddy Flux

The influence of different filter time constants in the data preprocessing detrending procedure was determined by calculation of the CO_2 flux for two days (14 time periods evenly scattered throughout each day) with various filter constants: 10 s, 25 s, 50 s, 100 s, 200 s, 400 s and not detrended (∞ s). The CO_2 flux of the selected time periods from Julian-day 242 (08/30) 17:00 PDT to Julian-day 243 (09/01) 17:00 PDT for the different detrending filter time constants is presented in

Figure A.1. Filtering out low frequencies due to detrending shows less effect during the second night from day 08/31 to 09/01 than for the night from 08/30 to 08/31. The influence of removing time scales larger than the filter time constant is apparent for both days during daylight period.

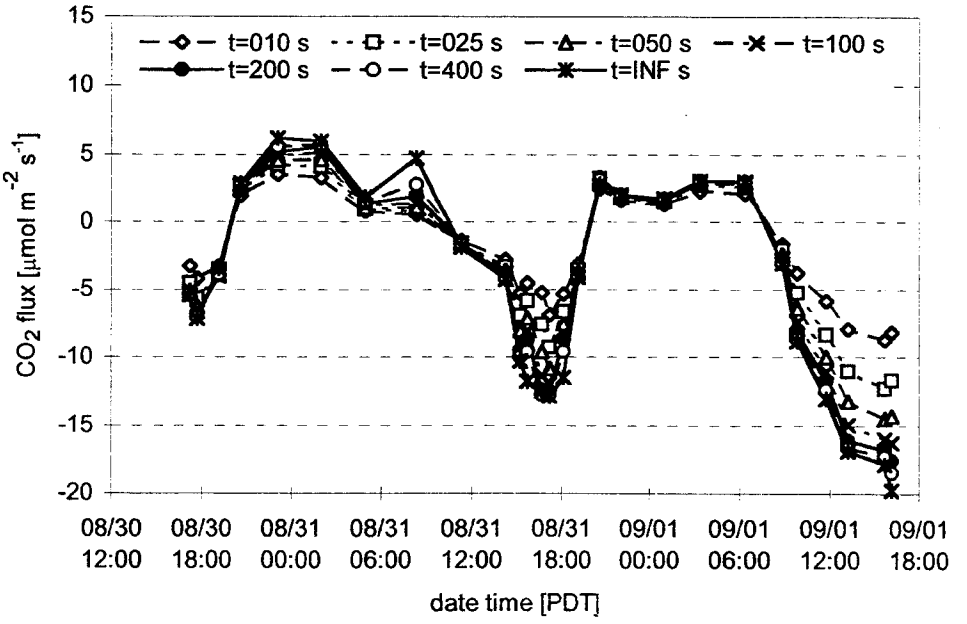

Figure A.1 Influence of the filter time constant used for detrending

For most midday cases, removing frequencies lower than 0.04 Hz (time scales larger than 200 s) does not have a major effect (less than 10 percent flux loss) for the CO_2 eddy flux calculations (see Figure A.2), suggesting that most of the CO_2 transport due to turbulence occurs on time scale smaller than 200 s. One exception occurred for the time period around 15:42 PDT on 08/31, when a reduction in the flux of more than 20 percent occurred for detrending with a 400 s filter constant (0.0025 Hz filter frequency), suggesting a covariance in the trend of the CO_2 signal and the wind speed on a large time scale. In most cases a flux contribution of about 40 percent is due to time scales between 200 and 10 seconds, about 50 percent is due to short time scales smaller than 10 seconds, and less than 10 percent contribution is due to non-turbulent trends with time scales longer than 200 s.

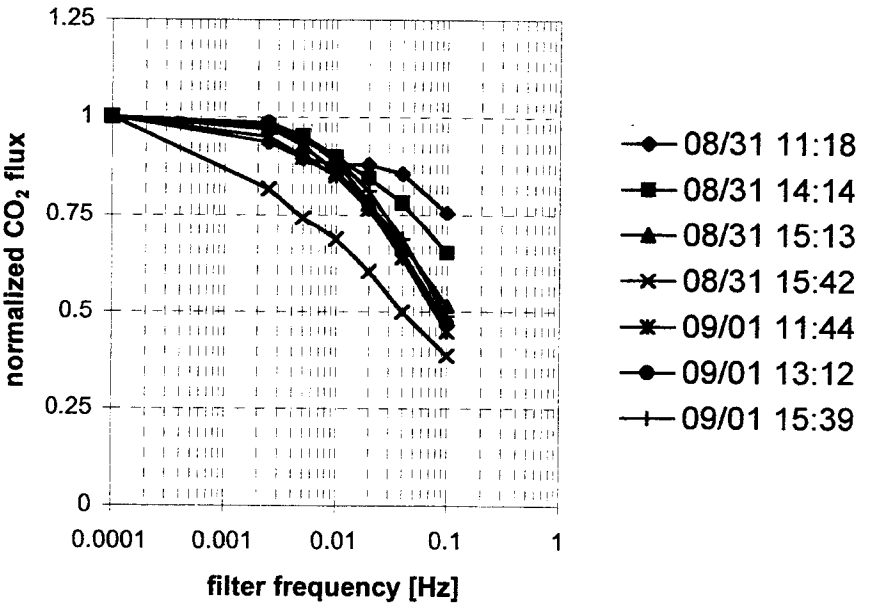

Figure A.2 Daytime: normalized CO_2 flux vs. filter frequency

For the night 08/30 to 08/31 (see Figure A.3) detrending had a stronger influence on the flux magnitude, than for the second night. The most likely cause for a large time scale trend during that time period is the shift of the wind direction from 320 ° to 240 °, which took place from 08/30 at 23:00 to 08/31 at 05:30. During the second night the wind direction stayed steady around 260 °.

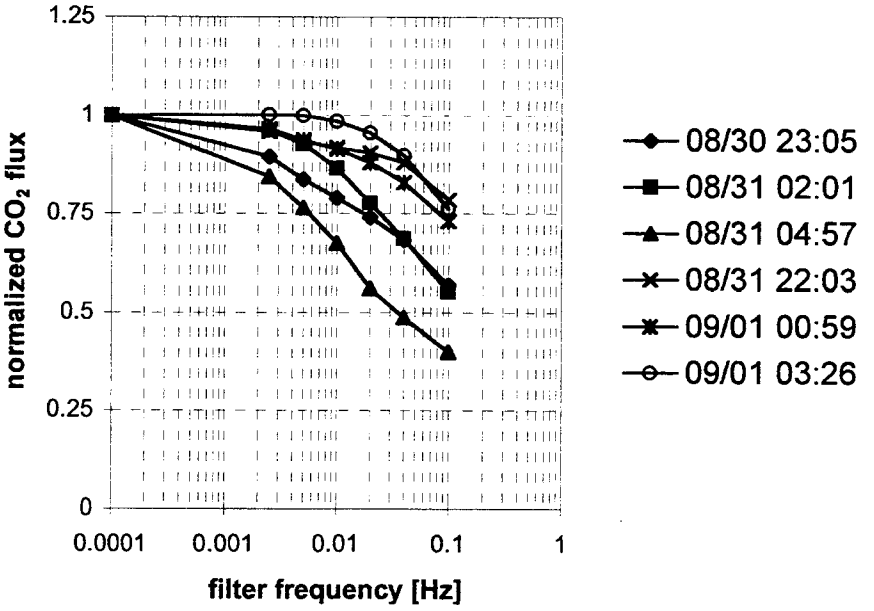

Figure A.3 Nighttime: normalized CO_2 flux vs. filter frequency

Appendix B Sonic Anemometer CO_2 Flux Comparison

For comparison with the fluxes calculated from the ATI sonic anemometer data, flux calculations were repeated for a few days with the Solent sonic anemometer as the source for the fast response wind speed data. The Solent was collocated with the ATI sonic on the walk-up tower boom with a separation of 0.5 m in the transverse direction.

Calculations were performed for the Julian-days 230, 231, 233 , 234, 235, 236, 241 to 247, 250, 261, and 262, resulting in a total of 808 calculated flux time periods. The standard screening applied to both ATI and Solent CO_2 flux data retains 342 of the 808 data points. The retained data points are shown in Figure B.1 and include cloudy and not-cloudy periods at the site.

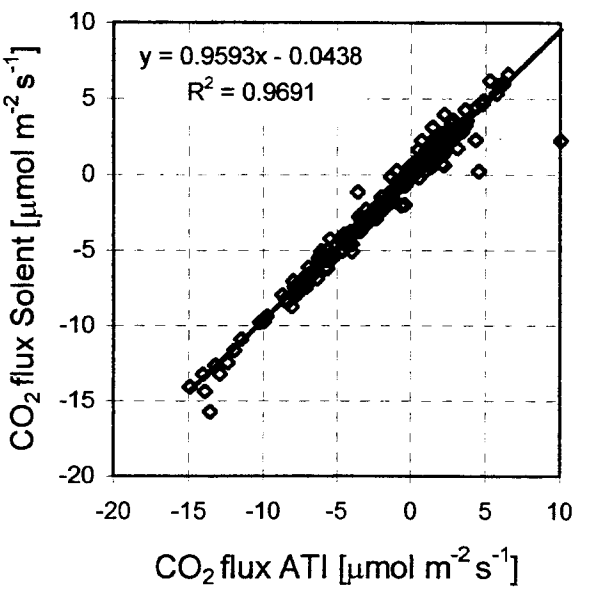

Figure B.1 Solent-ATI CO_2 flux comparison

An excellent agreement (r^2=0.97) is achieved between the two flux calculations (see Figure B.1). The flux calculated from the Solent underestimates the CO_2 flux from the ATI sonic by about 5%, which is probable related to the separation of the Solent sonic and the CO_2 sampling tube inlet, which leads to a reduction in the correlation of small eddies to the measured gas concentration.

Appendix C Sensitivity of Hourly Mean and Standard Deviation Flux Analysis to Missing Values for the High IPAR Vase

The hourly CO_2 flux for the days with high incident PAR are presented in Table C.1, hours, table cells, where missing data were filled-in, are shaded. The filling scheme was based on the simplified assumption of constant respiration during nighttime (00:00 to 06:00 and 20:00 to 24:00) and a linear trend for missing data during daylight (06:00 to 20:00) with adjacent flux values as starting and end value in the trend.

Table C.1 CO_2 flux [$\mu mol\ m^{-2}\ s^{-1}$] for Julian-days with high IPAR

PDT	225	227	230	235	241	244	247	249	255
0:30	7.00	4.14	0.69	6.14	0.81	1.22	0.52	0.50	0.35
1:30	7.04	3.86	0.69	5.97	1.32	1.13	0.52	0.50	0.35
2:30	7.04	6.15	0.69	5.80	0.79	1.96	0.52	0.50	0.35
3:30	7.04	5.11	0.69	5.64	0.79	1.89	0.52	0.50	0.35
4:30	7.04	5.06	0.69	5.92	1.55	1.81	0.52	0.50	0.35
5:30	7.04	3.28	0.89	4.52	1.15	1.94	0.52	0.50	0.35
6:30	3.39	2.62	1.09	4.37	1.41	2.39	0.52	0.50	-1.31
7:30	-0.25	2.83	1.29	0.51	0.90	0.66	1.75	-1.45	-2.98
8:30	-3.90	-0.22	0.68	-0.98	-0.11	-0.28	-0.09	-3.40	-4.64
9:30	-7.55	-2.60	-1.82	-1.62	-1.27	-2.94	-0.39	-5.35	-6.31
10:30	-11.20	-4.99	-6.02	-5.59	-4.83	-8.17	-3.39	-7.30	-7.97
11:30	-11.55	-7.38	-7.50	-7.93	-12.50	-10.40	-7.44	-9.25	-9.74
12:30	-11.85	-7.67	-11.40	-10.02	-10.35	-12.30	-13.00	-11.20	-14.20
13:30	-13.60	-7.97	-8.52	-9.98	-10.94	-13.50	-10.95	-7.79	-12.20
14:30	-12.30	-8.26	-8.27	-9.17	-9.39	-13.00	-12.45	-7.43	-9.96
15:30	-13.35	-9.43	-9.73	-11.40	-10.51	-12.65	-8.41	-4.94	-12.40
16:30	-11.20	-7.39	-7.74	-8.80	-11.60	-14.80	-8.63	-4.50	-9.77
17:30	-7.78	-3.54	-5.12	-6.21	-8.45	-7.69	-6.27	-3.28	-7.13
18:30	-4.35	-3.47	-5.26	-3.61	-5.30	-4.02	-3.91	0.04	-4.49
19:30	-0.92	-2.11	-1.88	-1.02	-2.15	-0.48	-1.56	0.93	-1.84
20:30	2.50	-0.45	0.31	1.58	1.00	0.32	0.80	0.65	0.80
21:30	2.50	1.76	0.58	1.58	1.00	0.52	0.80	1.31	0.80
22:30	2.50	1.55	0.70	1.58	1.00	0.16	0.80	1.56	0.80
23:30	2.50	1.51	1.01	1.57	1.00	1.13	0.80	0.84	0.80

The mean and standard deviation of each hour from all days with filled-in fields omitted (mean and stdev) and with filled-in values included ($mean_{filled}$ and $stdev_{filled}$) were calculated (see Table C.2). The sensitivity (S_{mean} and S_{stdev}) to the filling in of missing data was evaluated according to

$$S_{mean} = \left| \frac{mean - mean_{filled}}{0.5 * (mean + mean_{filled})} \right| \quad (50)$$

$$S_{stdev} = \left| \frac{stdev - stdev_{filled}}{0.5 * (stdev + stdev_{filled})} \right| \quad (51)$$

Table C.2 Sensitivity of mean and standard deviation calculation to filling in data at missing time periods

PDT	mean	stdev	$mean_{filled}$	$stdev_{filled}$	S_{mean}	S_{stdev}	$\lvert diff_{mean} \rvert$	$\lvert diff_{stdev} \rvert$
00:30	3.86	2.80	2.37	2.65	48%	5%	1.49	0.15
01:30	2.10	1.53	2.38	2.59	12%	51%	0.27	1.06
02:30	2.96	2.82	2.64	2.82	11%	0%	0.32	0.01
03:30	3.36	2.38	2.50	2.65	29%	11%	0.85	0.27
04:30	3.00	2.32	2.60	2.64	14%	13%	0.40	0.32
05:30	2.72	1.49	2.24	2.29	19%	43%	0.48	0.80
06:30	2.26	1.45	1.66	1.72	30%	17%	0.60	0.27
07:30	1.33	0.86	0.36	1.74	114%	67%	0.96	0.87
08:30	-0.16	0.53	-1.44	1.98	159%	116%	1.27	1.45
09:30	-1.61	0.92	-3.32	2.49	69%	92%	1.71	1.56
10:30	-6.74	2.59	-6.61	2.33	2%	11%	0.13	0.26
11:30	-9.25	2.01	-9.30	1.90	1%	5%	0.05	0.11
12:30	-11.79	1.38	-11.33	1.88	4%	31%	0.46	0.51
13:30	-10.93	2.14	-10.60	2.23	3%	4%	0.33	0.09
14:30	-9.85	1.91	-10.02	2.06	2%	8%	0.17	0.15
15:30	-10.31	2.60	-10.31	2.60	0%	0%	0.00	0.00
16:30	-9.45	3.13	-9.38	2.94	1%	6%	0.07	0.19
17:30	-4.91	2.03	-6.16	1.85	23%	9%	1.26	0.18
18:30	-3.18	2.27	-3.82	1.58	18%	36%	0.64	0.69
19:30	-0.88	1.41	-1.23	0.99	32%	35%	0.34	0.41
20:30	0.21	0.47	0.84	0.84	120%	57%	0.63	0.37
21:30	1.04	0.60	1.21	0.65	14%	8%	0.16	0.05
22:30	1.09	0.80	1.18	0.69	8%	16%	0.09	0.12
23:30	1.21	0.32	1.24	0.55	2%	54%	0.03	0.23

The sensitivity varies strongly with the number of missing data and time of day. The standard deviations for the filled-in case show less variance and are more homogenous between adjoining hours. The largest sensitivity is found for time periods with small flux magnitude.

The sensitivity to filling-in missing data for nighttime's with a substantial flux magnitude is in the range of 20 percent for the mean and 60 percent for the standard deviation. The obvious low mean and standard deviation for the hour 01:30 is likely caused by the screening procedure; the simple filling-in scheme adjusts the values into the same range as the mean and standard deviation of the adjacent hours.

The low number of missing data points for daylight hours results in a low sensitivity below 10 percent in the mean and standard deviation. Only the standard deviation for the time 12:30 shows a substantial increase in magnitude of about 30 percent, which is probable related to filling in a particularly small value.